Deciphering *Arabidopsis thaliana* Acclimation to Sublethal Combined Abiotic Stresses

Zhang Jiang[1], Ava Verhoeven[1] , Yihong Li[1], Romy Geertsma[1], Rashmi Sasidharan[1,*,†], Martijn van Zanten[1,*,†]

[1] Plant Stress Resilience, Institute of Environmental Biology, Utrecht University, Padualaan 8, 3584CH Utrecht, the Netherlands

[*] Corresponding authors: m.vanzanten@uu.nl, r.sasidharan@uu.nl

[†] Senior authors

Running title: Deciphering Acclimation To Combined Abiotic Stress

Abstract

Plants are frequently exposed to environmental challenges. Responses to sub-lethal abiotic stress combinations are complex and often distinct from responses to individual stresses and remain poorly understood. Investigating traits and molecular factors mediating acclimation to stress combinations is essential for the development of climate change-resilient field crops. Here, we studied the morphological, physiological, and molecular responses of *Arabidopsis thaliana* to i) co-occurring high temperature and drought and ii) flooding sequentially followed by drought, both of which have increased in frequency due to climate change. A set of 15 physiological and morphological traits were assessed during single and combined stresses. By combining these comprehensive trait analyses with transcriptome characterization, we established the generally additive effects of simultaneous or sequential stresses on plant morphology and physiology compared to the corresponding individual stresses. Although drought had a mild effect in both stress combinations, a unique transcriptome signature emerged upon combination with high temperature simultaneously or flooding sequentially. Molecular processes identified as important for multi-stress resilience included plastid-nucleus communication, ABA signaling and photo-acclimation. Based on the RNA-seq data, a set of 39 genes was identified as potential multi-stress response regulators. Mutants were tested to validate their contribution to plant survival and phenotypic acclimation under combined stress. We confirmed the involvement of several genes in regulating phenotypic acclimation traits. Among the novel identified factors are EARLY FLOWERING 6 (ELF6) and ARABIDOPSIS TÓXICOS EN LEVADURA (ATL80), with significant effects on plant growth, leaf development and plant survival (wilting) during high-temperature drought and post-submergence drought respectively.

Introduction

Increased occurrences of abiotic stresses such as heat, drought and flooding due to climate change are negatively impacting crop productivity (Kopecká et al., 2023; Shabbir et al., 2022) and thereby food security (Cushman et al., 2022; Kumar et al., 2022; Masson-Delmotte et al., 2021). Although the effect of such abiotic stresses on plant functioning has been extensively studied (Harb et al., 2010; Larkindale et al., 2005; van Veen et al., 2016) the focus has been predominantly on single stressors, often involving abrupt transfer of plants into harsh stressful conditions. In natural or agricultural settings, abiotic stresses seldom happen in isolation and usually occur at a sublethal severity (Bailey-Serres and Colmer, 2014; De Smet et al., 2021; Van Dooren et al., 2020; Zhang et al., 2020) with multiple stresses coinciding simultaneously or sequentially (Mittler, 2006; Suzuki et al., 2014).

Co-occurring stresses can elicit synergistic or antagonistic effects or are a blend of responses to individual stresses. Hence responsiveness cannot be simply deduced by taking the sum of the responses of individual stresses (Balfagón et al., 2019; Mittler, 2006; Rivero et al., 2022; Rizhsky et al., 2004; Suzuki et al., 2014; Zandalinas et al., 2020). For instance, high temperature induces stomatal opening to allow leaf cooling through transpiration, while under drought stomatal conductance is reduced to prevent unnecessary water loss. However, when high temperature and drought occur concurrently a signalling conflict occurs and the stomata tend to be closed (Mittler and Blumwald, 2010; Rizhsky et al., 2004; Zandalinas et al., 2016a, 2016b).

The precise acclimation strategy fitting a given stress combination is determined by various (sometimes limiting) parameters, such as plant genotype, developmental age, duration and severity of stresses (Rivero et al., 2022; Sinha et al., 2021; Zandalinas et al., 2021, 2016b; Zandalinas and Mittler, 2022; Zhou et al., 2017). Additionally, the sequence of events plays a pivotal role (Banti et al., 2008; Kong and Henry, 2016). For example, soil salinity pretreatment can alleviate effects of subsequent low-temperature damage in tomato plants, as salt stress-triggered signal cascades can activate downstream overlapping signal transduction pathways (*e.g.*, reactive oxygen species (ROS), abscisic acid (ABA) and low-temperature signaling) that enhance photosynthetic acclimation under low-temperatures (Yang et al., 2022).

Despite its importance, multi-stress acclimation mechanisms remain poorly understood (Rivero et al., 2022; Zandalinas et al., 2020; Zandalinas and Mittler, 2022). Here we characterized

69 the effects of two stress combinations typical of climate change in *Arabidopsis thaliana.* These
70 were: i) combined high temperature and drought and ii) submergence followed by drought, and
71 their corresponding individual stresses. A comprehensive assessment of the impact of these
72 stress combinations on plant morphology, physiology, and transcriptome revealed different, in
73 general additive, effects on plant growth, development and physiology compared to the
74 corresponding individual stresses. The unique phenotypic characteristics correlated with distinct
75 transcriptomic signatures involving synchronous regulation of multiple generic processes such as
76 plastid-nucleus communication (retrograde signaling), ABA signaling and photo-acclimation.
77 A reverse genetics approach was used to validate the contribution of a set of 44 candidate
78 genes to multi-stress acclimation responses. Effects were confirmed for several factors, including
79 FLOWERING 6 (ELF6) and ARABIDOPSIS TÓXICOS EN LEVADURA (ATL80) that impact on specific
80 subsets of traits related to growth, development and water status maintenance during high
81 temperature/drought or submergence/drought combinations. Our results reveal that acclimation
82 to different sublethal combinatorial stresses is likely coordinated by distinct candidate regulatory
83 genes acting as either positive or negative regulators of multi-stress acclimation traits.

84 ## Results

85

86 **Combined and sequential abiotic stresses elicit additive responses.**

87 *Arabidopsis* Columbia-0 (Col-0) plants were subjected to two different stress
88 combinations upon reaching the 10-leaf stage (LS10): i) high ambient temperature (27 °C) +
89 progressive drought (HTD) and ii) submergence, followed by progressive drought after de-
90 submergence (PSD; 21 °C) (Fig. 1A), control conditions (C; 21 °C) and corresponding single
91 stresses: high temperature (HT; 27 °C), submergence (S; 21 °C), whereafter plants were well-
92 watered during the post-submergence phase (PS) (Fig. 1A). Drought (D) was imposed
93 progressively by withholding watering. After 5 days, the average soil water content (%SWC)
94 dropped to 50–65% field water capacity (= 100% saturation), and to 30–40% after 10 days
95 (Supplemental Fig. S1, A and B). Plants subjected to HTD and PSD displayed earlier wilting than
96 when D was imposed in isolation (Supplemental Fig. S2, A-C) and produced fewer new leaves
97 than those subjected to the corresponding single stresses (Supplemental Fig. S2, D and E).
98 Drought-treated plants (D and PSD) showed increased chlorophyll content compared to the
99 relative controls (C and PS) (Supplemental Figs. S3 and S4). Based on these responses, we focused
100 on the 0, 5, 10 and 15 days following stress initiation time points in the remainder of this study
101 (Fig. 1A).

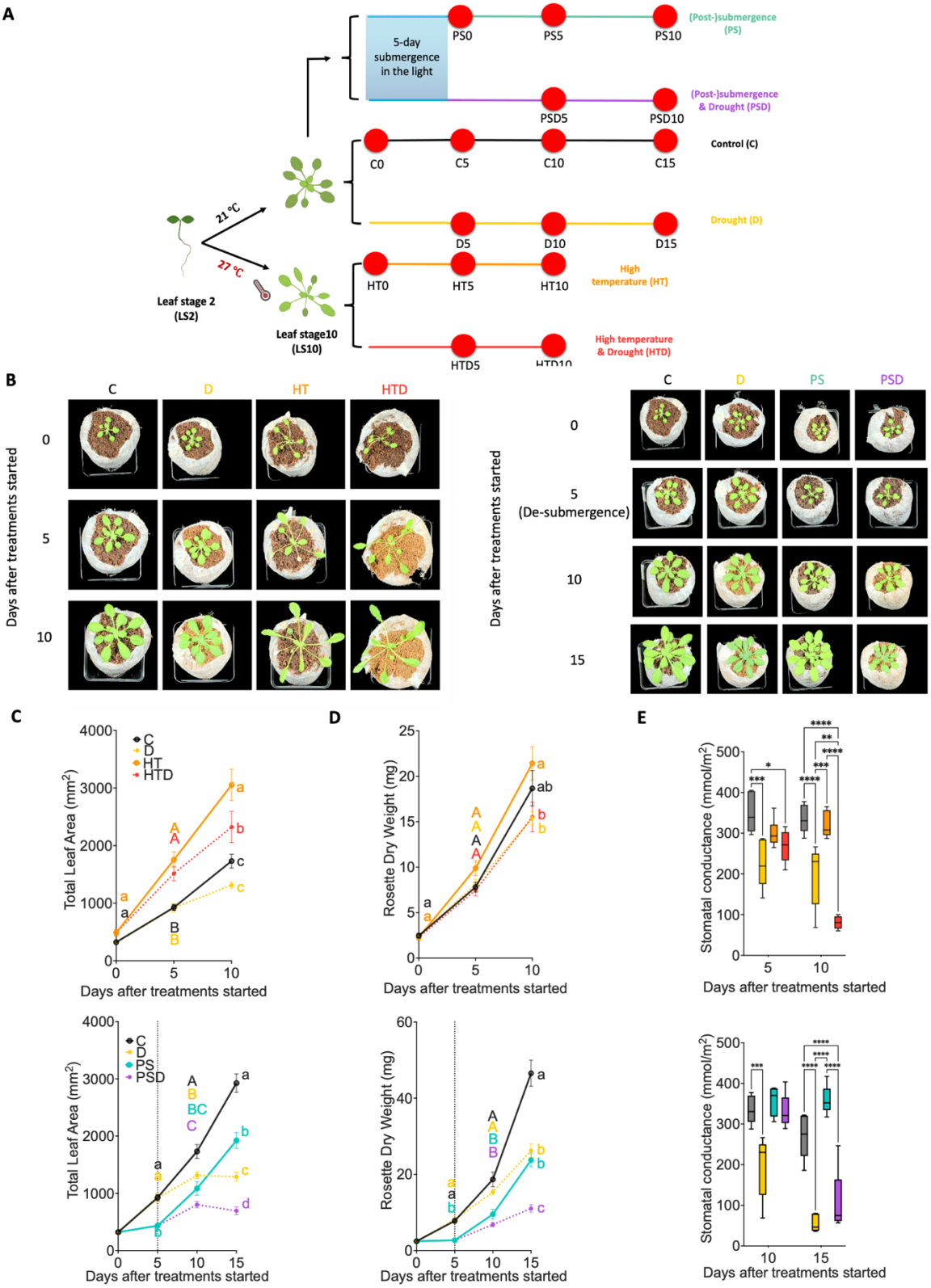
A
5-day submergence in the light
PS0
PS5
PS10
(Post-)submergence (PS)
PSD5
PSD10
(Post-)submergence & Drought (PSD)
C0
C5
C10
C15
Control (C)
D5
D10
D15
Drought (D)
HT0
HT5
HT10
High temperature (HT)
HTD5
High temperature & Drought (HTD)
21 °C
27 °C
Leaf stage 2 (LS2)
Leaf stage10 (LS10)
B
C
D
HT
HTD
Days after treatments started
0
5
10
PS
PSD
5 (De-submergence)
15
C
Total Leaf Area (mm²)
Days after treatments started
D
Rosette Dry Weight (mg)
E
Stomatal conductance (mmol/m²)

102

103

Figure 1. Effects of combined and sequential sublethal stresses and corresponding single stresses on phenotypic traits. (A) Experimental setup. Harvest moments and measurements (indicated by red dots) were typically at 0, 5, 10 and 15 (C and D) days after the drought (D, HTD and PSD) treatment started at average %SWC of 100%, 50–65%, 30–40% and ~20% respectively (Supplemental Fig. S1, A and B). For C, HT and PS the %SWC were maintained at the saturated level (95%-100%) across all timepoints. **(B)** Representative images of plants on Jiffy 7c coconut pellet growth substrate, subjected to combined (left) and sequential (right) stresses and the corresponding single stresses at 0, 5, 10 and 15 days, counted from the moment that the treatments started. **(C-E)** Total leaf area of the whole rosette (C, n = 14-20), rosette dry weight (D, n = 15-18) and stomatal conductance of young leaves (E, n = 5-6) of plants subjected to combined (upper row) and sequential (lower row) stresses and the relevant single stresses at the corresponding harvesting time points. Error bars indicate means ± SEM. Letters denote significant differences between different treatments at the same time points ($p < 0.05$, 2-way ANOVA with Tukey's Post-hoc test). The dashed vertical lines indicate the moment plants were de-submerged. Boxes indicate boundaries of the second and third quartiles (Q) of the data distribution. Black horizontal bars indicate median and whiskers Q1 and Q4 values within 1.5 times the interquartile range. Asterisks represent significant differences (*$p < 0.05$, **$p < 0.01$, ***$p < 0.001$, ****$p < 0.001$, 2-way ANOVA with Tukey's Post-hoc test). Abbreviations; C; control (black lines and symbols), D; drought (yellow), HT; high temperature (orange), HTD; high temperature & drought (red), S/PS; 5-day submergence / (post-)submergence & recovery (blue), PSD; (post-)submergence & drought (purple).

High temperature and drought

D did not significantly hamper rosette growth nor dry weight accumulation, but triggered primary root lengthening (Fig. 1, B-D; Supplemental Fig. S5D). Plants in HT showed the expected typical thermomorphogenic phenotype (Quint et al., 2016), including elongated petioles and hyponastic leaves (Fig. 1B; Supplemental Figs. S5, A-C and S6). HTD treatment resulted in smaller rosettes and shorter petioles and leaf blades compared with plants exposed to HT, but rosette size, petiole length and leaf blade length under HTD exceeded the values observed under D (Fig. 1C; Supplemental Figs. S5, B-C and S6). Plants grown in HT or D did not differ in dry weight compared to plants in C (Fig. 1D). However, HTD resulted in significant dry-weight reduction after 10 days compared to HT, but not C (Fig. 1D). Primary root length was significantly promoted in HTD compared to the individual stresses (Supplemental Fig. S5D). Together, this indicates that during the subjection to HTD, D and HT stresses interact.

Plants contained relatively more water under high temperature conditions (HT and HTD) than at control temperatures (C and D) (Supplemental Fig. S7A). Moreover, the differences in leaf surface temperature between 'control' and drought-treated plants at 27 °C (HT and HTD) were greater than at 21 °C (C and D) (Supplemental Fig. S7, B and C). Together with an accelerated drought-induced temperature increase at 27 °C compared to 21 °C (Supplemental Fig. S7, B and C), these results indicate that the drought effect on leaf temperature was more pronounced

123 when combined with high temperature. However, stomatal conductance of plants in C and HT
124 was not significantly different, whereas C and HTD did differ significantly, with HTD having lower
125 stomatal conductance (Fig. 1E). D caused, as expected, a reduction in relative water content
126 corresponding with a significant decline in stomatal conductance compared to C (Fig. 1E;
127 Supplemental Fig. S7A).

128 No differences in Malondialdehyde (MDA) content were observed across treatments up
129 to day 10 (Supplemental Fig. S7D), suggesting that no significant oxidative stress occurs. However
130 enhanced ion leakage in HT-treated plants (Supplemental Fig. S7E) points to membrane damage
131 at high temperatures (Nielsen et al., 1997; Sharma et al., 2012). The addition of 10-days drought
132 (HTD) tempered this effect, while no effect was observed when D was applied in isolation
133 (Supplemental Fig. S7E).

134

135 *Submergence and drought*

136 5-days complete submergence (S) led to severely inhibited rosette growth compared to
137 non-submerged plants (Fig. 1, B-D; Supplemental Figs. S8, S9 and S10). During post-submergence
138 plants could recover if irrigation was applied (PS) (Fig. 1, B-D; Supplemental Figs. S8, S9 and S10).
139 D had a significant negative effect on total rosette area and dry weight, compared to C after 10
140 days (Fig. 1, C and D). When D was imposed following de-submergence (PSD), total rosette area
141 and dry weight accumulation were further reduced compared to PS (Fig. 1, C and D; Supplemental
142 Fig. S10, A and E). In contrast to D, S restricted primary root lengthening whereas root elongation
143 was enhanced under PSD (Supplemental Figs. S8D and S10F).

144 D negatively affected relative water content after 15 days (Supplemental Fig. S11A),
145 which was enhanced under PSD (Supplemental Fig. S11A and S12A). Both D and PSD treatments
146 resulted in a reduction of stomatal conductance (Fig. 1E; Supplemental Fig. S12B). Accordingly,
147 leaf temperature was raised under these conditions (Supplemental Fig. S11, B-C).

148 Drought increased MDA accumulation, especially when combined with prior
149 submergence (PSD) (Supplemental Figs. S11D and S12C). Yet, no clear effect of PSD, D or PS was
150 observed on ion leakage (Supplemental Figs. S11E and S12D).

151

152 **Transcriptomic responses elicited by combined and sequential stresses**

153 Next, a comparative RNA-sequencing approach was taken using young leaves sampled 0,
154 5, and 10 days after stress initiation (Fig. 1A) to uncover molecular processes underlying
155 responses to combined and sequential stresses. In total, 58 samples, distributed over 15 different
156 harvesting timepoints were sequenced, resulting in 3,628,334,664 detected reads (Supplemental
157 Fig. S13A). On average, 72% of the mapped reads aligned to the Arabidopsis transcriptome (5.4
158 to 61.8 million reads per sample). For approximately one-third of sequenced samples less than
159 50% of the reads mapped to the Arabidopsis transcriptome (Supplemental Fig. S13A). 98.2% of
160 the unmapped reads were identified as RNA segments of *Arabidopsis Latent Virus 1* (ArLV1 RNA1
161 and RNA2; GenBank accessions MH899120.1 and MH899121.1, respectively) (Verhoeven et al.,
162 2023). Although this virus does not evoke visible symptoms in plants (Verhoeven et al., 2023),
163 viral infections could impact the host transcriptome (Shates et al., 2019). We therefore compared
164 samples with reads that mapped more than 50% with those mapping less than 50% to the
165 Arabidopsis transcriptome on day 5 C treatment (Supplemental Fig. S13B). No differentially
166 expressed genes between both fractions were detected, implying that ArLV1 does not
167 significantly impact the plant transcriptome.

168 PCA analysis revealed significant changes across time (PCO1, explaining 29,88% of
169 observed variation) and treatments (separated over PCO1 and PCO2) (Supplemental Fig. S14A).
170 As expected, individual biological replicates of the same timepoint and stress treatment clustered
171 together (Supplemental Figs. S14 and S15). Superimposing the fraction of reads mapping to the
172 Arabidopsis genome per sample on the PCA revealed no clear pattern (Supplemental Fig. S14B),
173 confirming that ArLV1 contamination did not significantly affect the transcriptome. We therefore
174 decided to continue processing our data using all samples except two (day 5 control) of which the
175 mapping percentages to Arabidopsis transcriptome were below 11% (Supplemental Figs. S13).

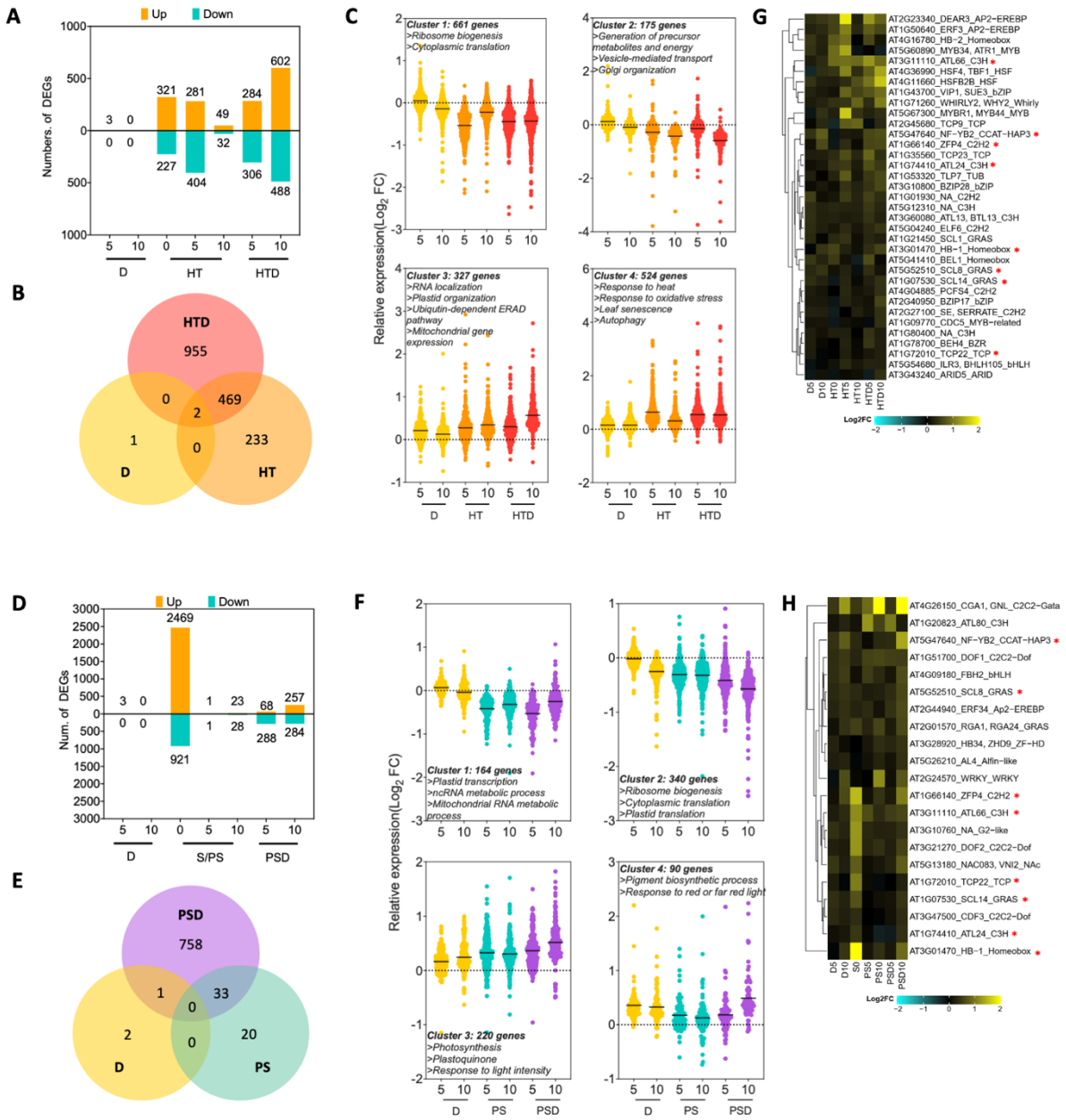

Figure 2. Effect of combined and sequential stresses and corresponding single stresses on the transcriptome. (A, D) Number of up- (orange) and down- (green) regulated DEGs (|Log_2FC| >0, $p < 0.05$) at day 0 (the pre-growth effect of HT before the drought treatment started), 5, and 10 days after the treatments (D) started (note HT was prolonged), compared to control (C) conditions. **(B, E)** Venn diagrams showing the number of DEGs commonly or differently detected in the combined (HTD), sequential (PSD) and single (D, HT, PS) stresses. **(C, F)** *k-means* clustering presenting expression patterns of identified DEGs at timepoints 5 and 10 days during combined or sequential stresses and the corresponding individual stresses. Violin plots indicate the distributions of relative expression (Log_2FC) of identified DEGs. Mean values of each violin plot are indicated by a solid black line. Dashed horizontal lines indicate Log_2FC = 0. Key enriched biological processes identified by Gene Ontology analysis and number of genes assigned to each cluster are listed above or below the graphs. **(G, H)** Hierarchically clustered heatmaps showing relative Log_2FC levels of transcription factors (TFs) (Supplemental Tables S3 and S4) identified among the upregulated DEGs in the HTD and PSD datasets. For each identified TF, the AGI gene locus ID, the commonly used abbreviation (if available) and TF family the factor belonged to, are listed. Color scales indicate Log_2FC values (relative to control (C) conditions). Red asterisks indicate overlapping TFs between HTD and PSD. For treatment abbreviations and used colors, see legend of Figure 1.

176 **High temperature and submergence alter transcriptome responses to drought**

177

178 *High temperature and drought*

179 In response to D, only 3 differentially expressed genes (DEGs; $|Log_2FC| > 0$, FDR < 0.05)
180 were detected; *GUARD-CELL-ENRICHED GDSL LIPASE 3* (*GGL3*), *PHOSPHOFRUCTOKINASE 1* (*PFK1*)
181 and *AT5G16990* (Fig. 2A). Under HTD, the drought effect became more apparent (590 and 1090
182 DEGs after 5 and 10 days of HTD, respectively) (Fig. 2A). Moreover, HTD resulted in 955 unique
183 DEGs that were not detected under D or HT (Fig. 2B). Thus, combined stress evokes a unique
184 transcriptomic response and has greater impact than individual stresses. HT and HTD shared 469
185 DEGs, suggesting that HT has a more dominant effect on the transcriptome than D in the
186 combined stress (HTD) situation (Fig. 2B). Only 2 DEGs; *PFK1* and *AT5G16990,* were commonly
187 regulated by D, HT and HTD (Fig. 2B), suggesting that these genes might be involved in early stress
188 responses in young leaves.

189 *K-means* clustering of the 1687 detected DEGs (day 5 and 10) across individual and
190 combined stress treatments revealed 4 groups with distinct expression patterns (Fig. 2C). Cluster
191 1 and 2 consisted of DEGs downregulated under HT and HTD conditions and unchanged under D.
192 Gene Ontology (GO) annotation revealed that these clusters were dominated by genes associated
193 with ribosome activities and protein processing (Fig. 2C; Supplemental Table S1). DEGs that were
194 upregulated in HT and HTD were in Cluster 3 and 4 (Fig. 2C). These DEGs are associated with RNA
195 processing (particularly alternative splicing), organelle activities including ubiquitin-depended
196 endoplasmic-reticulum-associated protein degradation (ERAD) pathway, mitochondrial activities
197 and stress responsiveness such as response to heat, starvation or oxidative stress and leaf
198 senescence (Fig. 2C; Supplemental Table S1).

199

200 *Submergence and drought*

201 To characterize the effects of submergence followed by drought (PSD), the following
202 comparisons (Log_2FC in gene expression) were made: i) 5-day submergence (S) compared to pre-
203 submergence (submergence effect), ii) 5 or 10 days of D compared to C (drought effect), iii) 5- or
204 10-day PS or PSD compared to C respectively, to determine effects of S followed by irrigation (PS)

205 or drought (PSD). This approach ensured comparisons between samples at similar developmental
206 stages.

207 5-days submergence resulted in 3390 DEGs (2469 up- and 921 downregulated) (Fig. 2D),
208 reflecting considerable transcriptome reconfiguration. Following de-submergence (PS) only a
209 limited number of DEGs were detected after 5 and 10 days (2 and 51 DEGs respectively; Fig. 2D).
210 Upregulation of several core-hypoxia responsive genes (Mustroph et al., 2009) during 5 days S
211 pointed to occurrence of tissue hypoxia (Supplemental Fig. S16). As expected, the upregulation
212 was reversed by re-oxygenation following de-submergence (PS and PSD at day 5 and 10)
213 (Supplemental Fig. S16). D during de-submergence (PSD) resulted in 356 and 541 DEGs at 5 and
214 10 days of PSD, respectively (Fig. 2D). Like HTD, PSD also led to a unique transcriptomic signature,
215 as the majority of DEGs identified after PSD treatment (758 DEGs) were not affected by PS nor D
216 (Fig. 2E). Only 33 DEGs were shared between PSD and PS (Supplemental Fig. S17).

217 *k-means* clustering including all 814 DEGs (day 5 and 10 across D, PS and PSD treatments;
218 Fig. 2F), revealed four clusters. Two clusters contained genes downregulated by PS and PSD
219 (Cluster 1 and 2) and two contained genes upregulated in these conditions (Cluster 3 and 4) (Fig.
220 2F; Supplemental Table S2). GO analysis revealed that Cluster 1 and 2 were dominated by genes
221 associated with nucleic acid, ribosome and translation-related processes. Several of the
222 downregulated GO terms in clusters 1 and 2 were associated with plastid functions, indicating
223 impeded chloroplast activities during post-submergence (PS and PSD). In Cluster 3
224 photosynthesis-related GO terms were significantly enriched, while in Cluster 4 only two GO
225 categories were enriched (Fig. 2F; Supplemental Table S2). Of note, *CYTOKININ-RESPONSIVE GATA*
226 *FACTOR 1* (*CGA1*/*GNL*) was shared between these two GO groups.

227

228 **Transcription factors mediating acclimation to combined and sequential stresses**

229 In total, 48 different transcription factors (TFs) from 23 TF families were upregulated by
230 HTD (35) or PSD (21), with 8 TFs overlapping between the two groups (Fig. 2, G and H;
231 Supplemental Fig. S18). Only 7 out of 35 HTD-upregulated TFs were also upregulated under HT
232 (Supplemental Table S3) and only 2 out of 21 PSD-upregulated TFs, were induced under 5- or 10-
233 day PS (Supplemental Table S4). This underscores the unique response that is evoked by
234 combined stress application. Considering PSD, of the 19 uniquely induced TFs, 12 were

235 significantly upregulated by 5-day S (Supplemental Table S4). This points to a large effect of prior
236 submergence on the sequential-stress transcriptome signature.
237 Gene regulatory networks (GRNs) were constructed with the HTD and PSD upregulated
238 gene clusters (Clusters 3 and 4) to identify putative regulatory nodes (Supplemental Fig. S19, A
239 and B). The obtained HTD network consisted of 12913 interactions between 847 regulators
240 (nodes). Only 4169 interactions between 340 regulators were formed in the PSD network
241 (Supplemental Fig. S19, A and B). To identify putative 'master regulators', 11 nodes with the
242 highest number of connections with the other regulators in the same GRN were selected. Four of
243 these were shared between the HTD- and PSD- networks: *G-BOX BINDING FACTOR 3* (*GBF3*),
244 *ABSCISIC ACID RESPONSIVE ELEMENT-BINDING FACTOR 1* (*ABF1*), *ABA INSENTITIVE 5* (*ABI5*) and
245 *NF-YB2* (Supplemental Fig. S20, Table). Note that *THYLAKOID LUMEN PROTEIN* (*TLP18.3*) ranked
246 12th in the degree analysis but is associated with chloroplast function (Järvi et al., 2016; Wu et al.,
247 2011). *GENOMES UNCOUPLED 4* (*GUN4*) and *AT1G66130* had the same number of nodes in GRN,
248 therefore in total 11 overrepresented genes for HTD and PSD are indicated in Supplemental Fig.
249 S19.
250
251 **Validation of identified candidate genes by mutant analysis**
252 Next, a reverse genetics approach was taken to validate the effects of identified factors on
253 multi-stress acclimation (Supplemental Table S5). For this, TFs were selected that were
254 upregulated during either HTD or PSD, supplemented with some of the overrepresented genes
255 from the GRNs. In total, 41 confirmed homozygous T-DNA insertion mutants, covering in total 39
256 candidate genes (28 for HTD and 19 for PSD) , were obtained (Supplemental Tables S6 and S7).

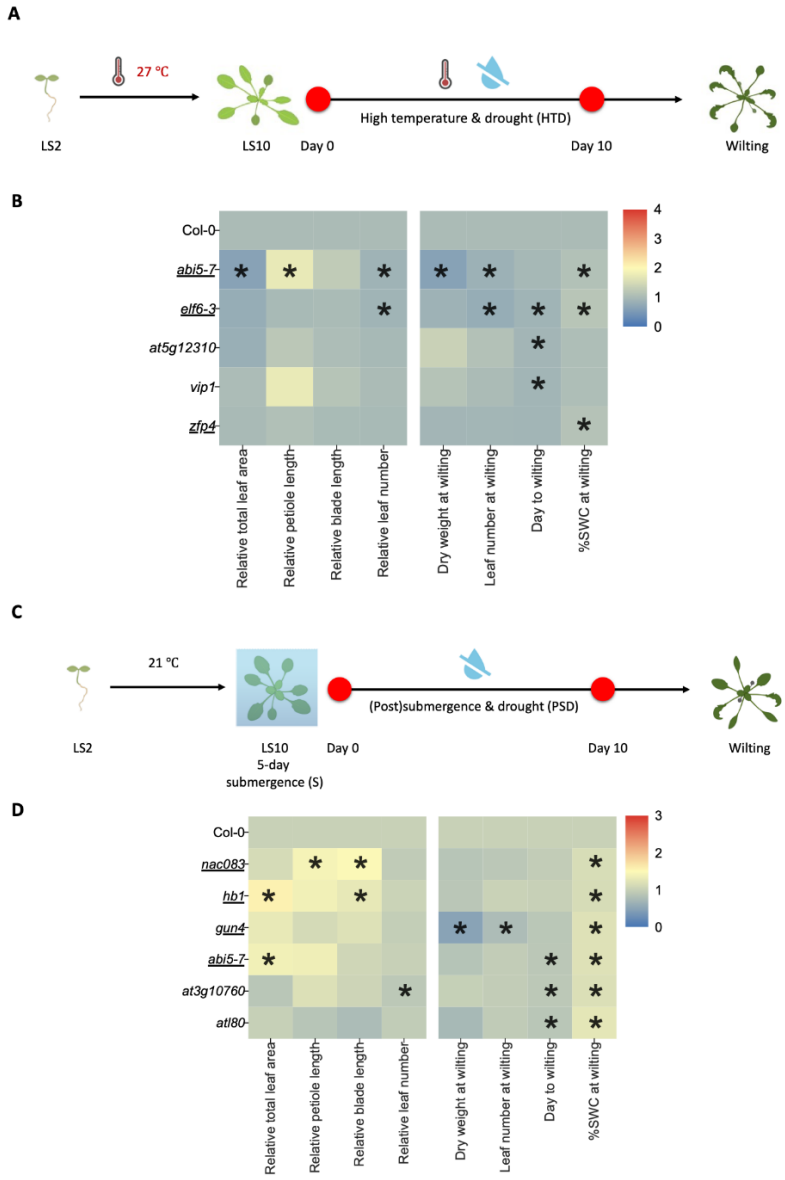

Figure 3. Plant growth, development and wilting traits of selected mutants under combined or sequential stresses. (A, C) Experimental scheme for the used reverse genetic analyses. 2-leaf stage (LS2) Arabidopsis mutants and corresponding wild-type (WT) plants were pre-grown at 27 °C (HTD; A) or 21 °C (PSD; C) until they reached the 10-leaf stage (LS10). Subsequently, the plants were subjected to 10 days of combined high temperature and drought conditions (HTD), or 5-day submergence in the light, followed by 10-day drought treatment (PSD) and thereafter were both left unwatered until wilting occurred. Measurements of phenotypic traits were carried out at day 0, day 10 and at the moment of wilting (*i.e.*, timepoint differed per plant). **(B, D)** Heatmaps indicating phenotypic traits of Arabidopsis mutants with either significantly advanced wilting time and/or high %SWC at wilting, relative to the corresponding wild-type plants (Col-0) during the exposure to HTD (B) or PSD (D). The relative values of total leaf area, petiole/blade length and leaf number were calculated by normalizing the data obtained at day 10 by that of day 0 (left four columns in each panel). Dry weight and leaf number at wilting, days to wilting and %SWC at wilting are indicated in the right four columns per panel). The abbreviated names of tested mutants and the wild type plants are indicated per row. Color scales indicate relative values of measured traits (relative to the corresponding wild-type Col-0 plants). Underlined mutants indicate confirmed knockout of the corresponding genes based on previous studies (Supplemental Tables, S6 and S7). Asterisks represent significant differences between mutants and wild-type plants for the particular trait (Supplemental Tables S8 and S9) ($p < 0.05$, unpaired t-test). n=8-12.

257 *High temperature and drought*

258 Traits indicative of plant growth and development were measured at 0 and 10 days after
259 stress initiation. Subsequently, the stress treatment was extended until the plants showed wilting
260 symptoms (Fig. 3A). Of the 29 mutants with putative effect on HTD traits (Fig. 3A; Supplemental
261 Table S6), *aba insensitive 5* (*abi5-7*), *early flowering 6* (*elf6-3*), *at5g12310*, *VIRE2-interacting*
262 *protein 1 (vip1)* and *zinc finger protein 4* (*zfp4*) displayed early wilting phenotypes (Fig. 3B;
263 Supplemental Table S8). As expected, the ABA signaling mutant *abi5-7* (Bi et al., 2017; Dekkers et
264 al., 2016) showed substantially deviating phenotypes under HTD compared to the wildtype (WT)
265 in addition to clear wilting phenotypes (Fig. 3B; Supplemental Table S8). This points to a pivotal
266 role for ABA signaling in modulating plant growth and development under HTD. The *elf6-3* mutant
267 showed accelerated wilting (Fig. 3B; Supplemental Table S8) and a considerable delay in leaf
268 initiation rate.

269

270 *Submergence and drought*

271 Of the 20 mutants tested (Fig. 3C; Supplemental Table S7), six (*NAC domain containing*
272 *protein 83* (*nac083*), *homeobox1* (*hb1*), *gun4*, *at3g10760*, *abi5-7* and *arabidopsis tóxicos en*
273 *levadura* (*atl80*)) exhibited early wilting phenotypes under PSD (Fig. 3D; Supplemental Table S9).
274 The *nac083*, *hb1* and *abi5-7* mutants exhibited a significant increase in total leaf area and/or leaf
275 length (Fig. 3D; Supplemental Table S9). Both *gun4* and *at3g10760* showed reduced leaf initiation
276 rates. Notably, *gun4* weighed only ~50% of the (dry) weight at the moment of wilting compared
277 to WT (Supplemental Table S9). Despite wilting at a high %SWC level, *atl80* mutant phenotypic
278 traits were comparable to WT (Fig. 3D; Supplemental Table S9).

279 For mutants exhibiting early wilting during HTD (*elf6-3*, *at5g12310*, *vip1* and *zfp4*) or PSD
280 (*atl80, nac083, at3g10760, hb1, gun4*), experiments were extended with inclusion of the
281 corresponding individual stresses (Fig. 4 and Fig. 5; Supplemental Figs. S20, S21, S22 and S23).
282 The *abi5-7* mutant was omitted as ABA signaling is already studied in great detail in plant
283 acclimation to diverse stresses (Skubacz et al., 2016; Wang et al., 2021).

284 *Validation of high temperature and drought mutants*

285 Compared to WT, the *elf6-3* mutant had higher dry weight and rosette area under HTD
286 treatment (Fig. 4, B and C). This mutant also displayed enhanced dry weight and had a larger

287 rosette area at 0-day (pre-growth) at HT, but neither at later HT time points nor under C and D
288 treatments (Fig. 4, B and C). This indicates that ELF6 is a negative regulator of plant growth and
289 rosette expansion under HTD. The *zfp4* mutant showed reduced dry weight and total leaf area
290 under 0- day HT and 10- day D, whereas *vip1* only showed a smaller total leaf area than the WT
291 under 0- or 10- day HT (Fig. 4, B and C). This suggests that both ZFP4 and VIP1 mediate plant
292 growth during D and/or HT but not HTD.

293 In HTD, all mutants with accelerated wilting displayed a significant decrease in chlorophyll
294 content (Supplemental Fig. S21A). In contrast, both *vip1* and *at5g12310* displayed higher
295 chlorophyll content under 10-day D (Supplemental Fig. S21A). No significant differences in
296 chlorophyll abundance were observed between mutants and WT during HT single treatment
297 (Supplemental Fig. S21A). Under HT and HTD, stomatal conductance of all mutants was
298 comparable to WT (Supplemental Fig. S21B). Notably, 5-day D significantly reduced stomatal
299 conductance in both *vip1* and *at5g12310* mutants compared to WT (Supplemental Fig. S21B).
300
301

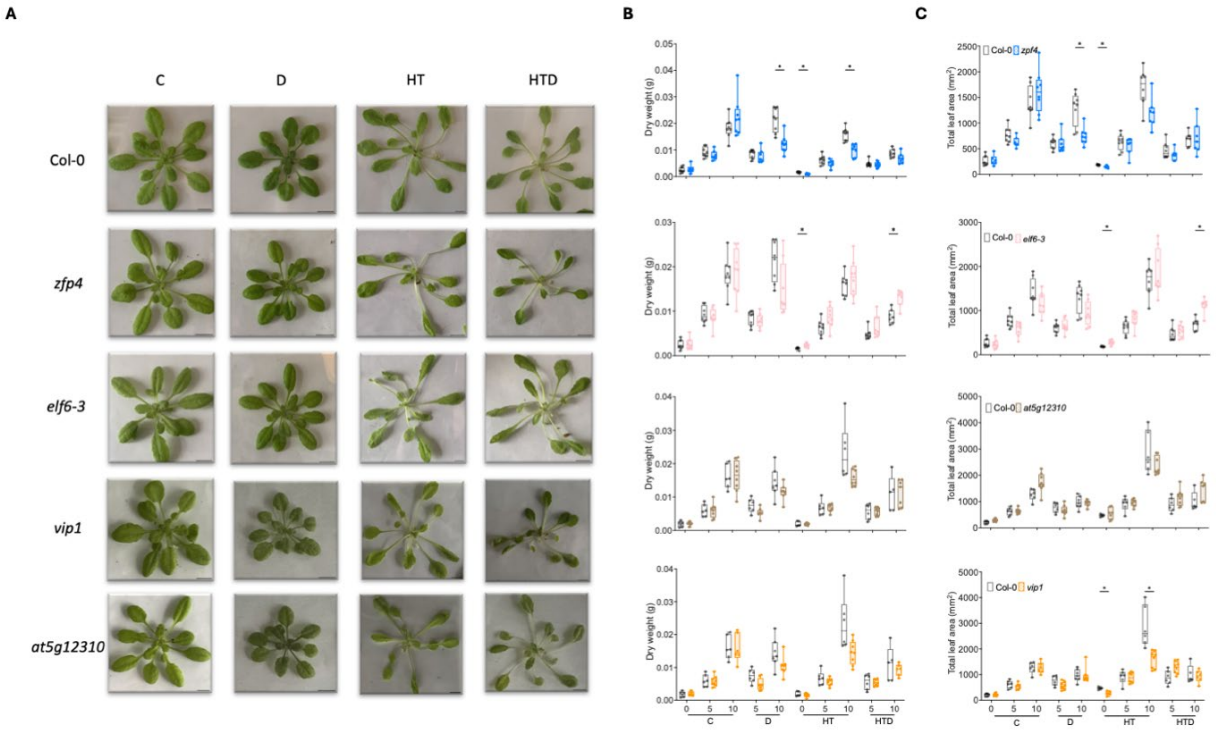

302

Figure 4. Effect of combined and individual stresses on phenotypic traits of selected Arabidopsis mutants. (A) Representative images of whole rosettes of selected mutants and corresponding wild-type plants (Col-0) grown on Jiffy 7c coconut pellet substrate, subjected to single and combined stresses at 10 days after the treatments initiated. Scale bars indicate 1 cm. **(B, C)** Rosette dry weight (B) and total leaf area (C) of Arabidopsis mutants (*zfp4* (blue), *elf6-3* (pink), *at5g12310* (brown), and *vip1* (orange)) and the wild-type plants (Col-0; gray). For plants that wilted before the harvesting time points, traits were measured at the day of wilting onset. Boxes indicate boundaries of the second and third quartiles (Q) of the data distribution. Horizontal bars indicate median and whiskers Q1 and Q4 values within 1.5 times the interquartile range. Asterisks represent significant differences between the mutant and the corresponding wild-type plants within the same time point ($p < 0.05$, multiple unpaired t-test with Holm-Šídák correction). Numbers indicate days after treatments started. For treatment abbreviations and used colors, see legend of Figure 1. n= 5-10.

Validation of post-submergence and drought mutants

The *atl80* mutant exhibited decreased dry weight and total leaf area compared to the WT when subjected to PSD and developed smaller rosettes and shorter leaves during C and D treatment (Fig. 5, A-C; Supplemental Fig. S22, A and B). Both *nac083* and *hb1* mutants had similar dry weights and total leaf area as the WT during individual (D, PS) and sequential stresses (PSD) (Fig. 5, B and C). However, prolonged PS treatment resulted in decreased blade length and leaf number in *nac083* (Supplemental Fig. S22, B and C). As reflected by reduced dry weight accumulation, blade length and leaf number during 10-day PS, the *at3g10760* mutant was unable to recover to the same extent as WT after submergence (Fig. 5B; Supplemental Fig. S22, B and C). The *gun4* mutant appeared highly sensitive to D and PS, as dry weight, total leaf area, leaf length and leaf initiation rate were significantly reduced (Fig. 5, B and C; Supplemental Fig. S22, B and C). However, *gun4* also exhibited a significant reduction in these traits under C (Fig. 5, B and C; Supplemental Fig. S22, B and C). Chlorophyll content and stomatal conductance remained unchanged for most mutants (Supplemental Fig. S23, A and B), except *gun4,* which had higher chlorophyll and stomatal conductance under 10-day C (Supplemental Fig. S23A).

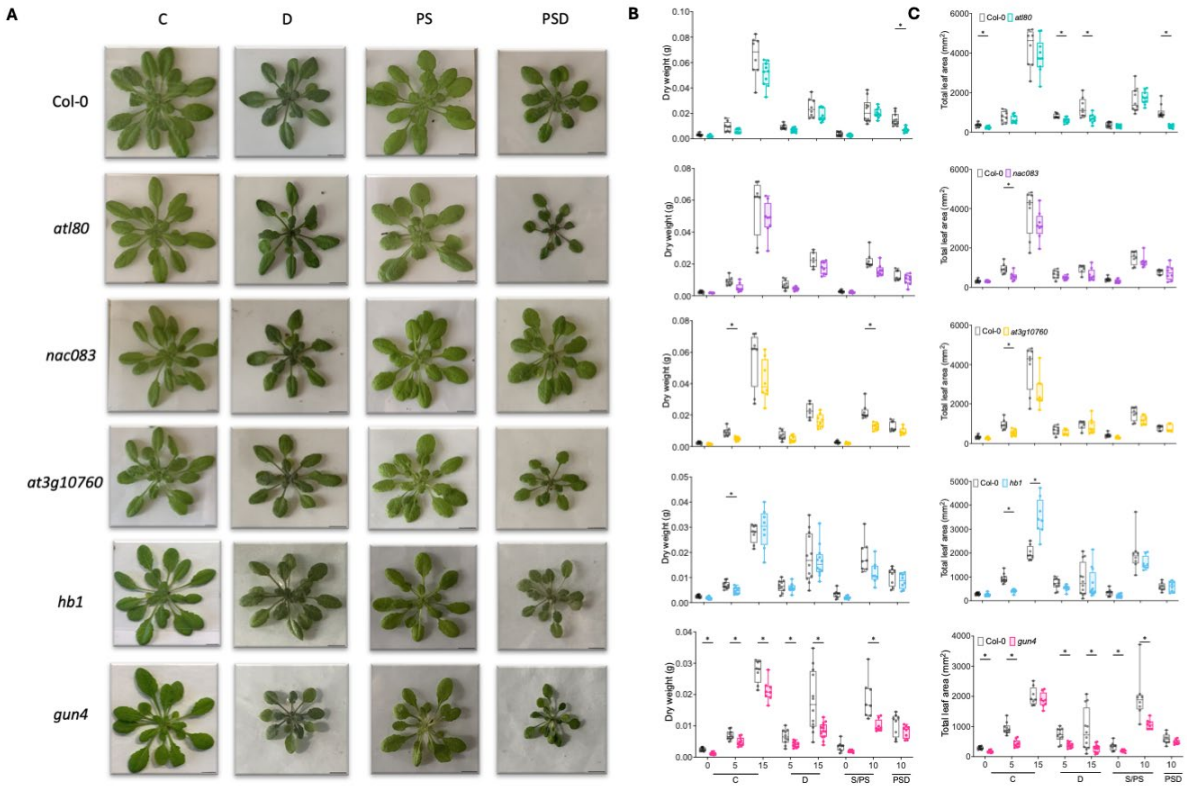

Figure 5. Effect of sequential and individual stresses on phenotypic traits of selected Arabidopsis mutants. (A) Representative images of whole rosettes of selected mutants and the corresponding wild-type plants (Col-0) grown on Jiffy 7c coconut pellet substrate, subjected to single and sequential stresses 15 days after the treatments started. Scale bars indicate 1 cm. **(B, C)** Rosette dry weight (B) and total leaf area (C) of Arabidopsis mutants (*atl80* (aqua), *nac083* (purple), *at3g10760* (yellow), *hb1* (azure) and *gun4* (magenta)) and the wild-type plants (Col-0; gray). For plants that wilted before the harvesting time points, the traits were measured on the day of wilting onset. Boxes indicate boundaries of the second and third quartiles (Q) of the data distribution. Horizontal bars indicate median and whiskers Q1 and Q4 values within 1.5 times the interquartile range. Asterisks represent significant differences between the mutant and the corresponding wild-type plants within the same time point ($p < 0.05$, multiple unpaired t-test with Holm-Šídák correction). Numbers indicate days after treatment started. For treatment abbreviations and used colors, see legend of Figure 1. n=6-13.

Principal component analysis reveals trait correlations and validates mutant effects

A PCA analysis incorporating all measured traits of all mutants and WTs revealed strong correlation between leaf development traits (including relative petiole (RPL) and blade (RBL) length and total leaf area (RLA)) (Fig. 6, A and B). Likewise, relative leaf number (RLN), leaf number at wilting (LNW) and relative dry weight at wilting (DWW) were positively correlated (Fig. 6, A and B). As expected, days to wilting (DTW) and %SWC at wilting (%SWCW) negatively correlated (Fig. 6, A and B), indicating that fast-wilting mutants indeed also generally contained a high %SWC at the moment of wilting.

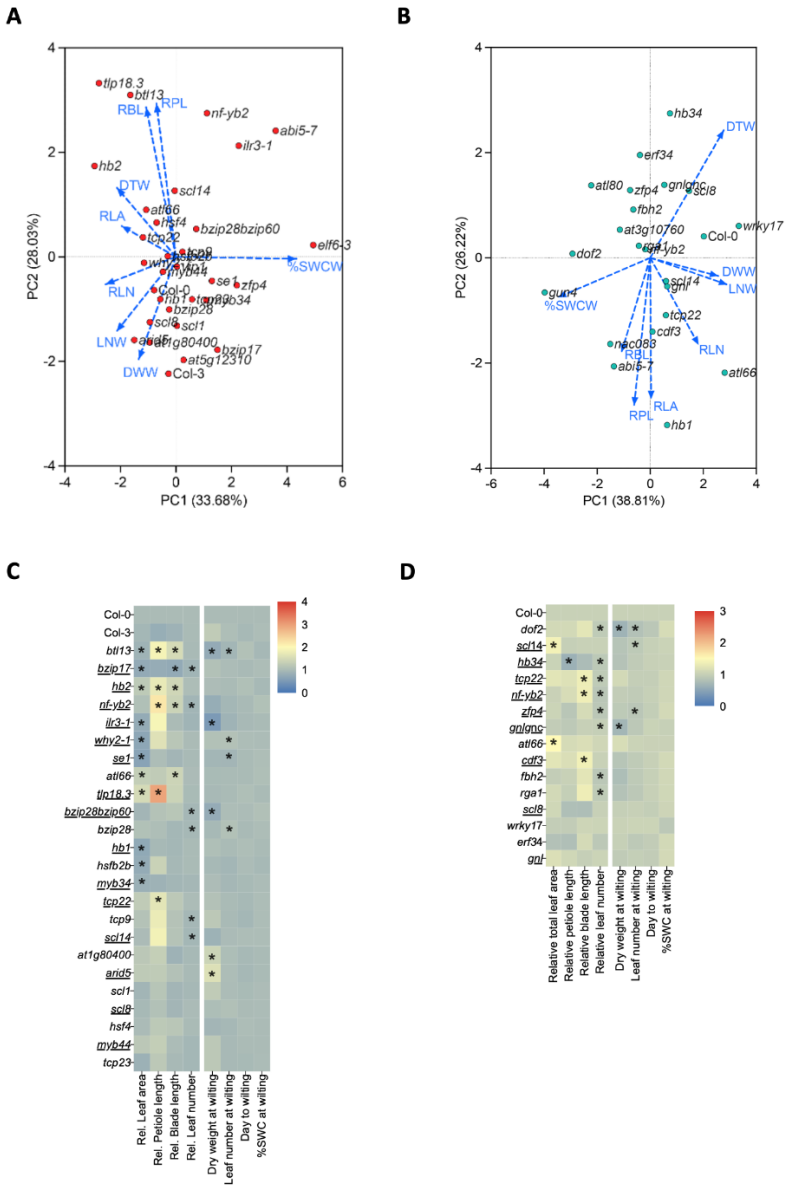

Figure 6. Plant growth, development and wilting trait analyses of selected mutants under combined or sequential stresses. (A, B) Principal component analysis (PCA) of all measured traits of all tested mutants and corresponding wild-type plants subjected to HTD (A) or PSD (B). Visualized are the distributions of mutants and wild-type plants indicated by symbols and correlations between measured traits by arrows. Abbreviations of traits: RLA: relative total leaf area, RPL: relative petiole length, RBL: relative blade length, RLN: relative leaf number, DWW: dry weight at wilting, LNW: leaf number at wilting, DTW: days to wilting, %SWCW: percentage of soil water content (%SWC) at wilting. **(C, D)** Heatmaps indicating phenotypic traits of mutants without early wilting phenotypes (opposed to those indicated in Fig. 3 and Fig. 4) along with the corresponding wild-type plants (Col-0 and Col-3) in response to HTD (C) or PSD (D). Relative values of total leaf area, petiole/blade length and leaf number were calculated by normalizing the data obtained at day 10 by that of day 0 (left four columns). Dry weight and leaf number at wilting, days to wilting and %SWC at wilting are indicated in the (right four panels). Abbreviated names of mutants and the wild-type plants are indicated per row. Color scales indicate relative values of measured traits (relative to the corresponding wild-type plants, with Col-3 relative to Col-0). Underlined mutants indicate confirmed knockout mutants of the corresponding genes based on previous studies (Supplemental Tables S6 and S7). Asterisks represent significant differences between mutant and the corresponding wild-type plants for the particular trait (Supplemental Table S8 and S9) ($p < 0.05$, unpaired t-test), n=8-12. For treatment abbreviations and used colors, see legend of Figure 1.

330

331 *High temperature and drought*

332 The *tlp18.3* and *bca2a zinc finger atl13* (*btl13*) mutants, correlated with leaf lengthening
333 traits under HTD treatment and displayed significantly increased (young) leaf lengthening
334 compared to WT (Col-0 or Col-3) (Fig. 6, A and C; Supplemental Table S8). For example, *tlp18.3*
335 recorded a relative petiole length that was approximately 3-fold higher than Col-0 (Fig. 6C;
336 Supplemental Table S8). A similar trend was observed for *homeobox 2* (*hb2*), *nf-yb2*, *arabidopsis*
337 *tóxicos en levadura* (*atl66*) and *teosinte branched1 /cycloidea/proliferating cell factor 22* (*tcp22*)
338 mutants, exhibiting enhanced relative petiole and/or blade elongation (RPL and RBL) under HTD
339 (Fig. 6, A and C; Supplemental Table S8). The mutants *btl13*, *why2-1* and *serrate* (*se-1*) showed
340 reduced total leaf area and leaf number at wilting compared to the WT (Fig. 6C; Supplemental
341 Table S8).

342 The basic region/leucine zipper motif (bZIP) TFs, bZIP17 and bZIP28 proteins have been
343 implicated in heat stress responses (Gao et al., 2022; Kataoka et al., 2017). Compared to the WT,
344 *bzip17* displayed significantly reduced total rosette area, blade lengthening and leaf formation
345 under HTD, while *bzip28* had reduced leaf number (Fig. 6C; Supplemental Table S8). The *bzip28*
346 *bzip60* double mutant (Samperna et al., 2021), showed a significant delay in both leaf formation
347 and dry weight accumulation (Fig. 6C; Supplemental Table S8). *ilr3-1* mutant plants exhibited
348 strongly enhanced hyponastic growth when grown at elevated ambient temperature (27 °C),
349 whereas additional drought during high temperature (HTD) did not further alter this phenotype
350 (Supplemental Fig. S24, A and B). Next to these observations, several mutants displayed
351 significant changes in only one of the measured traits (Fig. 6C; Supplemental Table S8). Notably,
352 *ilr3-1* phenotypically resembled *abi5-7* (Fig. 6, A and C).

353 *Post-submergence and drought*

354 The *DNA binding with one finger 2* (*dof2*) mutant showed reduced leaf formation rate and
355 dry weight accumulation in PSD (Fig. 6D; Supplemental Table S9). The *scl14* mutant showed
356 increased total leaf area, whereas leaf number at wilting was reduced (Fig. 6D; Supplemental
357 Table S9). Interestingly, *hb34*, which displayed decreased petiole length and leaf formation rate,
358 exhibited a typical leaf-rolling phenotype in PSD, but not under C (Fig. 6D; Supplemental Fig. S25,
359 A and B). Additionally, *tcp22* and *nf-yb2* mutants had significantly longer leaf blades but reduced

leaf initiation rates (Fig. 6D; Supplemental Table S9). The *zfp4* mutant only showed a lag in leaf formation in PSD (Fig. 6D; Supplemental Table S9). The single *gnl* mutant (Richter et al., 2013) had no clear phenotype (Fig. 6D, Supplemental Table S9). However, in combination with a knockout of the *GNL* homolog, *GATA NITRATE-INDUCIBLE CARBON-METABOLISM INVOLVED* (*GNC*) (*gnlgnc*) reduced dry weight and impaired leaf initiation were noted (Fig. 6D; Supplemental Table S9). Additionally, both *atl66* and *cycling dof factor 3* (*cdf3*) mutants had larger leaves (Fig. 6D; Supplemental Table S9). The *flowering bhlh 2* (*fbh2*) and *repressor of ga1-3 1* (*rga1*) mutants showed a significant reduction in relative leaf number compared to the WT when exposed to PSD (Fig. 6D; Supplemental Table S9).

Discussion

Co-occurring abiotic stresses often have distinct effects on plants and elicit different acclimation responses compared to individual stresses (Choudhury et al., 2017; Nadeem et al., 2023; Zandalinas and Mittler, 2022; Zhang and Sonnewald, 2017). In addition, (combined) abiotic stresses encountered in natural or agricultural conditions are often at a gradual or sublethal severity, and hence relatively mild, compared to those reported in experimental laboratory studies (Morales et al., 2022; Zhang et al., 2020)

The experimental system that we present in this work departed from standard protocols of abrupt stress exposures. Arabidopsis plants were exposed to sublethal single and combined stresses, that typify weather events exacerbated by climate change. Our comprehensive dataset reveals a suite of unique phenotypic and molecular signatures of plant responses that emerge only when these sub-lethal stresses are applied sequentially or simultaneously (Fig. 1, C-E, Fig. 2, A and D; Supplemental Figs. S5, S7, S8, S10 S11 and S12). These responses are also highly dependent on the duration and sequence of stress imposition (Guo et al., 2021). For instance, many studies have explored the combined effects of heat and drought, but with varying results. For example, a predominant drought signature was noted on plant growth and development when heat and drought were applied concurrently (Zhou et al., 2017). In addition, in wheat (*Triticum aestivum*), episodes of prolonged drought in combination with heat waves exacerbate biomass reduction and loss of grain yield, when compared to individually applied drought or heat (Perdomo et al., 2015; Pradhan et al., 2012; Tricker et al., 2018). This is attributed to the negative interactions between heat and drought, with the effects becoming additive when combined (Suzuki et al., 2014). Additionally, a meta-analysis using >120 published cases studying crop responses to combined heat and drought revealed that it caused on average twice the decrease in relative yield (to control) compared to exposure to heat stress alone (Cohen et al., 2021). In apparent contrast, in our study, HT had a dominant effect over D on plant rosette growth and leaf development (Fig. 1, B-D; Supplemental Figs. S5 and S6). This is likely because in our experiments HT was applied from germination onwards, well before D was applied.

Submergence significantly hampered plant growth but did not cause plant death (Fig. 1, B-D; Supplemental Figs. S8, S9 and S10). This is likely because our flooding treatment occurred

399 under the regular day/night regime, which differs from studies where lethality was noted using
400 submergence in darkness (Van Veen et al., 2013; Vashisht et al., 2011). Plants were able to steadily
401 recover if optimal irrigation was applied following de-submergence (Fig. 1, B-D; Supplemental Figs.
402 S8, S9 and S10). However, when experiencing drought following de-submergence (PSD), leaf
403 lengthening, rosette area increase and dry mass accumulation were significantly impacted (Fig. 1,
404 B-D; Supplemental Figs. S8, S9 and S10). This is in line with Luo et al. (2009) who highlighted the
405 essential role of photosynthetic acclimation during submergence recovery (Luo et al., 2009). As
406 drought can be a major impediment to photosynthesis (Chaves et al., 2009; Cornic, 2000), the
407 observed inhibition of growth and development could be explained by hampered photosynthetic
408 acclimation. Interestingly, phenotypic differences between PS and PSD were greater than those
409 between C and D after 10 days (Supplemental Fig. S10). This implies that PS exerted a negative
410 synergic effect on D in regulating plant growth and development in the PSD treatment.

411 Although both HT and PS interact with D and consequently elicit distinct effects on plant
412 phenotypes under the combined stress conditions, HT and PS seemingly affect physiological
413 responsiveness to HTD and PSD to different degrees. For example, when combined with HT,
414 drought-promoted leaf temperature increase occurred substantially earlier than under individual
415 drought conditions (Supplemental Fig. S7, B and C). In contrast, a submergence pre-treatment (S)
416 did not accelerate drought-induced leaf temperature elevation (Supplemental Fig. S11, B and C).
417 Furthermore, stomatal conductance decreased 5 days after HTD (Fig. 1E), but not during 5-day
418 PSD (Fig. 1E; Supplemental Fig. S12B). A likely explanation is that stomata are highly susceptible
419 to high temperature, resulting in a pronounced stomatal response when combined with drought
420 (De Smet et al., 2023).

421 Drought can have a major impact on the transcriptome (Bouzid et al., 2019; Chen et al.,
422 2021). However, while our plants clearly experienced drought (Fig.1, B-D; Supplemental Fig.S1
423 and S2), D did not elicit significant transcriptomic changes (3 DEGs, Fig.2, A and D) nor evoked
424 strong effects on phenotypic traits shortly after stress initiation (Fig. 1, B-D; Supplemental Figs.
425 S5, S6, S8, S9 and S10). This is consistent with a study by Prasch & Sonnewald in which only 41
426 DEGs were identified after 5-day progressive drought treatment (Prasch and Sonnewald, 2013).
427 The relatively mild drought intensity likely explains the limited number of DEGs (Clauw et al.,
428 2015). In addition, the young leaves that were sampled may be less responsive to drought than

429 for instance roots tissues, as plants might evoke protective mechanisms to prioritize stress
430 protection of younger leaves and meristematic tissues (Rankenberg et al., 2024, 2021; Verelst et
431 al., 2013).

432 In line with observed unique responses at the phenotypic level, combinatorial stresses
433 imposed distinct and more profound effects on the transcriptome compared to single stress
434 application (Fig. 2; Supplemental Fig. S14). For both stress combinations we observed a
435 considerable number of unique multi-stress specific DEGs. Notably, the majority of PSD-triggered
436 DEGs were not affected by PS nor D (Fig. 2, D and E). This difference in transcriptome
437 reconfiguration is consistent with the concept that prior exposure to one stress can have
438 consequences for the response to the second stress (Rejeb et al., 2014).

439 Our RNA-seq dataset permitted the identification of genes putatively contributing to
440 morpho-physiological responses to combinatorial and/or individual stresses. To identify these
441 candidate genes, we focused on upregulated TFs and regulatory hubs identified from constructed
442 GRNs (Fig. 2, G and H; Supplemental Fig. S19; Supplemental Table S5). 39 candidate genes
443 identified in this way were experimentally validated to probe their functions in combinatorial
444 stress acclimation. The aim was to unveil genetic effects based on testing a broad range of
445 candidate factors, rather than focusing on deciphering the precise molecular mechanisms
446 underlying selected genes. This approach admittedly neglects downregulated genes, which might
447 also play important roles in mediating responses to combined and/or sequential stresses and are
448 worthwhile to test in future experiments.

449 We identified *ELF6* as a negative regulator of phenotypic acclimation to HTD, while *ATL80*
450 is a positive regulator for PSD (Fig. 3, B and D, Figs. 4 and 5; Supplemental Figs. S20 and S22). *ELF6*
451 and its close homolog *RELATIVE OF EARLY FLOWERING 6* (*REF6*), function as histone H3 at Lys27
452 trimethylation (H3K27me3) demethylases in Arabidopsis (Crevillén et al., 2014; He et al., 2022;
453 Lu et al., 2011). H3K27me3 is crucial for the regulation of plant thermomorphogenesis and heat
454 stress memory (Casal and Balasubramanian, 2019; Perrella et al., 2022; Yamaguchi et al., 2021).
455 Therefore, the involvement of *ELF6* in regulating plant growth and development under HTD may
456 connect to H3K27me3-mediated high temperature responses. ATL80 is a plasma membrane-
457 localized RING E3 ubiquitin ligase that negatively regulates cold stress response and phosphate
458 mobilization (Suh and Kim, 2015). ATL80 was recently found to potentially target components

within the retrograde signaling pathways for degradation (Méndez-Gómez et al., 2024). Additionally, we identified regulators such as *ZFP4* and *GUN4*, as factors in controlling plant wilting under HTD or PSD. *ZFP4* and *GUN4* appear to participate in rosette expansion and/or dry weight accumulation under individually applied stresses such as D, HT and PS, but not combinatorial stresses (Fig. 3, B and D, Figs. 4 and 5; Supplemental Figs. S20 and S22). Further investigations are needed to decipher their precise roles in controlling (combinatorial) stress acclimation.

Conclusions

From the observed diversity in affected phenotypic traits across the tested mutants, treatments and timepoints (Fig 3, B and D, Fig. 6), we conclude that different aspects of acclimation strategies of plants to deal with HTD or PSD, are coordinated by a multitude of genetic factors. These factors together determine certain phenotypic outcomes depending on developmental (st)age and relative stress levels. For example, in response to HTD, TFs such as TLP18.3, BTL13, TCP22 and HB2 are likely involved in orchestrating leaf elongation, possibly as negative regulators, as their corresponding mutant lines displayed induced relative leaf lengthening (Fig. 6, A and C). Upon PSD treatment, HB1 and CDF3 seemingly inhibit the lengthening of petiole and blade (Fig. 6, B and D).

Altogether, our work contributes to a better understanding of plant response to sublethal combinatorial stresses. Generated insights can contribute to the establishment of mechanistic models for predicting trait responsiveness under the given stress condition. In addition, it should be investigated how sublethal combinatorial stresses affect productivity in agronomical crops, and whether the multitude of identified multi-stress regulators also contribute to resilience of commercial crops. Such investigations are critical considering the increased co-occurrence of these stresses in the context of climate change. This work has therefore the potential to contribute to breeding and/or engineering of field crops that maintain optimal yields in future climate conditions.

487 ## Materials and methods

488

489 **Plant materials, growth conditions and stress treatments**

490 Arabidopsis Col-0 seeds were sown on Primasta potting soil (Asten, The Netherlands) and
491 stratified 4 days in darkness. Plants were grown in MD1400 (Snijders, The Netherlands) climate
492 chambers under 8h photoperiod, 21 °C or 27 °C (day and night), 130-150 µmol m^{-2} s^{-1} PAR with
493 fluorescence tube or LED lightening and 70% RH. Plants that reached the 2 true-leaf stage were
494 transplanted to Jiffy 7c coconut pellet substrate (Jiffy Products International BV, Zwijndrecht, The
495 Netherlands) that were pre-soaked in water and 50 mL Hoagland solution (Millenaar et al., 2005)
496 (saturated weight = 250±20 g), contained in 9x9 cm pots for stability. Additional Hoagland solution
497 was supplied 2, 5 and 7 days after transplantation. Every second day, water was added and pots
498 were randomized to account for position effects.

499 Plants containing 10 true leaves (LS10) were subjected to sublethal stress conditions two
500 hours after the photoperiod started or remained in control conditions (C/HT). Progressive drought
501 (HTD/D) consisted of withholding watering. Drought severity, expressed as relative soil water
502 content (%SWC), refers to the ratio between the measured pellet weight and weight at full field
503 capacity (Supplemental Fig. S1, A and B). Plants subjected to submergence (PS and PSD) were pre-
504 grown and treated at 21 °C. One day before treatment initiation, plastic tubs (54 x 27 x 37 cm)
505 were disinfected with a chlorine tablet (Diversey Inc., Racine, USA) and thereafter rinsed. The
506 tubs were filled with deionized water and allowed to equilibrate to the climate room's
507 temperature. Plants were completely submerged (S) for 5 days while receiving the regular
508 day/night treatment. Thereafter, the pellets containing the plant were covered by absorbent
509 papers to remove excess water until the weight was comparable to non-submerged control (C)
510 and were then either subjected to the regular regime of irrigation (PS), or to progressive drought
511 conditions by withholding watering (PSD).

512

513 **Morphological analyses**

514 To assess leaf angles the two most hyponastic intermediate-aged leaves were imaged after
515 placement perpendicular to a camera. Plant shoots were thereafter detached, flattened using
516 transparent paper, and imaged from the top. ImageJ software (National Institutes of Health, USA)

517 was used to determine leaf traits. For hyponasty, leaf angle relative to the horizontal was
518 measured by taking the average angle of the captured opposing leaves.
519 To quantify dry weight, plants were dried in an oven set at 80 °C and weighed on an
520 analytic balance (Sartorius BP221S, Göttingen, Germany). To quantify leaf initiation (rate), the
521 number of all visible leaves (excluding cotyledons), was scored daily. Primary root length was
522 determined using a ruler, after the pellet substrate was rinsed from the roots with tap water.
523
524 **Physiological trait analyses:**
525 Chlorophyll content was determined using a CCM-300 Chlorophyll Content Meter (Opti-
526 Sciences Inc., Hudson, USA). After calibration, the detector was placed at 5 mm distance from the
527 leaf and chlorophyll content was calculated based on the fluorescence intensity. For destructive
528 biochemical detection, chlorophyll was extracted from detached leaves using 96% DMSO.
529 Absorption was determined at 664, 647 and 750 nm wavelengths using a spectrophotometer
530 plate reader (Synergy HT Multi-Detection Microplate Reader; BioTek Instruments Inc., USA). Dry
531 weight of the remaining plant material was used to calculate relative chlorophyll a, b, and total
532 chlorophyll content.
533 Relative water content was calculated as (Fresh weight–dry weight)/(turgor weight–dry
534 weight))x100%. To this aim, fresh weight of excised rosettes was determined using an analytic
535 balance (Sartorius BP221S, Göttingen, Germany). The rosettes were then immediately allowed to
536 saturate with water in petri dishes (24 hours in darkness). Excess water was removed and turgor
537 weight of plants was measured. Plants were then dried at 80°C and dry weight was recorded.
538 Stomatal conductance was measured of the abaxial leaf side using an SC-1 Leaf Porometer
539 (Decagon Devices, Inc., Pullman, USA) equilibrated to ambient temperature.
540 Leaf surface temperatures were recorded using a FLIR A655sc LWIR thermal imaging
541 camera (Teledyne FLIR, USA) with a 13.1 mm FoV 45° x 33.7° hawkeye IR lens. Thermal images
542 were captured every 15 minutes using FLIR ResearchIR Max 4 software (Teledyne FLIR, USA) from
543 the start of the stress treatments till wilting occurred. Temperatures of 6 leaves per plant were
544 measured at ZT = 0, 6, 12, 18 h and every 4th image, equaling every 24 hours, the regions of
545 interest was adjusted to correct for leaf growth and movement.

546 To determine Malondialdehyde (MDA) content, detached rosettes were grinded in
547 ethanol after recording fresh weight and cold-centrifuged. Part of the supernatant was mixed
548 with an equal volume of TCA/TBA solution (0.65% (w/v) thiobarbituric acid in 20% (w/v)
549 trichloroacetic acid). The mixture was shaking-incubated at 95°C for 30 minutes and cooled in an
550 ice bath. After cold-centrifugation, absorbance was measured using a spectrophotometer plate
551 reader (Synergy HT Multi-Detection Microplate Reader; BioTek Instruments Inc., USA) at 532 and
552 600 nm. MDA concentration was calculated and normalized by fresh weight: MDA (nmol/mL) =
553 ((A532-A600)/155000)x1000000
554 For quantification of ion leakage, rosettes were detached, placed in a tube containing
555 deionized water and shaken by rolling (1 hour at RT). Initial conductivity was measured using a
556 pre-calibrated EC-33 conductivity meter (HORIBA, Japan). The samples were then incubated at
557 95°C for 30 minutes and cooled down to RT, after which final conductivity was measured. Ion
558 leakage was calculated as: Ion leakage=(Initial conductivity/final conductivity)x100%.
559
560 **Transcriptomics sample preparation and analysis**
561 The 7th-10th leaves counted from the earliest emerged true leaves at LS10 were flash-
562 frozen in liquid nitrogen and kept at -80 °C. Samples were grinded using a cryogenic grinding mill
563 (Retsch, Haan, Germany) and plant total RNA was extracted using the RNeasy kit (Qiagen,
564 Germany) following the manufacturers protocol.
565 RNA quality control, library construction and sequencing were performed by Macrogen
566 (Amsterdam, The Netherlands). RNA integrity and purity were determined using an Agilent
567 Technologies 2100 Bioanalyzer (Agilent Technologies, Palo Alto, USA) and only samples with
568 Integrity Number of 7 or above were used for library construction by the TruSeq stranded mRNA
569 protocol (Illumina, USA). Libraries were sequenced using an Illumina Novaseq6000 sequencer
570 (Illumina, USA) with 150 bp pair-end reading. Generated datasets were deposited at the NCBI
571 Gene Expression Omnibus (Project ID: PRJNA863409).
572 Data processing (trimming, read filtering and mapping) and differential gene expression
573 analysis were conducted as previously described (Verhoeven et al., 2023). Two samples with a
574 total mapped Arabidopsis read count below 7 million due to *ArLV1* infection were removed. For
575 the determination of *ArLV1* effects on plant transcriptome, control (C) samples at timepoint 5

576 days were selected, as three of these samples contained relatively few reads mapping to *ArLV1*
577 (0.01-9.56%) and four samples contained high amounts of *ArLV1* (78.94- 90.08%). Only for this
578 analysis, the complete dataset including the two low-quality samples was used.

579 Statistical analysis was done in R using the log_2-normalized TPM values in linear models
580 ran for 5 and 10 days timepoints separately, with different stress treatments as variables
581 compared to the control treatment at the same timepoint. Obtained significances were corrected
582 using a Benjamini-Hochberg adjustment (provided by the *prcomp* function). Expressed genes
583 were visualized by ggplot2 (Wickham, 2009).

584 *k-means* clustering was used to arrange the significantly regulated genes in clusters with
585 similar expression patterns. The optimal number of clusters was determined visually by plotting
586 the within-cluster sums of squares and the average silhouette with the fviz_nbclust function from
587 the factoextra package in R (Lê et al., 2008). Groups with a high variation in expression between
588 the stress treatments were chosen for additional enrichment analysis.

589 For the GO enrichment analysis, Metascape (Metascape, http://Metascape.org/) (Zhou et
590 al., 2019) was used with settings of p value cutoff = 0.01, minimal number of overlapping genes
591 = 3 and a minimal enrichment value = 1.5.

592 The locus IDs of Arabidopsis were inputted into Arabidopsis transcription factor database
593 (AtTFDB, https://agris-knowledgebase.org/AtTFDB/) and TFs were automatically identified by
594 annotating the candidates to TFs from 50 different TF families. Candidate gene IDs were first
595 imported into TF2Network (Kulkarni et al., 2018) to search for promoter binding sites and
596 thereafter putative upstream TFs were identified. These TFs were then analyzed for co-expression
597 and protein-DNA interactions with the predicted targets and the networks thereafter generated
598 using Cytoscape (Shannon et al., 2003).

599

600 **Confirmation of T-DNA insertion lines**

601 gDNA was extracted from leaves using the Direct PCR-Phire and Phusion kit (Thermo
602 Scientific, Inc, USA) following the manufacturers protocol. Presence of T-DNA insertions and
603 homozygosity were determined by PCR (primers see: Supplemental Tables S6 and S7). We were
604 unable to obtain homozygous lines for 12 genes, mainly because of issues with seed germination
605 of obtained seed stocks.

Statistical analysis

If not explicitly mentioned otherwise, figures were generated using GraphPad Prism 9 (GraphPad Software, La Jolla, USA) or Biorender.com. Statistical analyses were performed using GraphPad Prism 9 or R software. Significance was calculated using an alpha of 0.05.

Acknowledgements

We thank Rens Voesenek and Sjef Smeekens for their support in the early stages of the project. Evelien Stouten, Alejandro Morales and Basten Snoek are thanked for their technical support and advice.

Funding

This research was funded by China Scholarship Council (CSC) grant 201806170025 to Z.J. and Nederlandse Organisatie voor Wetenschappelijk Onderzoek (NWO) grant 867.15.031 to R.S. and M.v.Z

Author contributions

ZJ, AV, RS, MvZ, designed the research; ZJ, AV, YL, RG performed research. ZJ, AV, RS, MvZ, analyzed data; ZJ, RS, MvZ wrote the paper.

Conflict of interest

The authors declare no conflict of interest.

Accession numbers

Generated sequence datasets from this article were deposited at the NCBI Gene Expression Omnibus (Project ID: PRJNA863409).

632 **References**

633

634 • Bailey-Serres, J., Colmer, T.D., 2014. Plant tolerance of flooding stress – recent advances. Plant,
635 Cell & Environment 37, 2211–2215. https://doi.org/10.1111/pce.12420
636 • Balfagón, D., Sengupta, S., Gómez-Cadenas, A., Fritschi, F.B., Azad, R.K., Mittler, R., Zandalinas,
637 S.I., 2019. Jasmonic Acid Is Required for Plant Acclimation to a Combination of High Light and
638 Heat Stress. Plant Physiol. 181, 1668–1682. https://doi.org/10.1104/pp.19.00956
639 • Banti, V., Loreti, E., Novi, G., Santaniello, A., Alpi, A., Perata, P., 2008. Heat acclimation and
640 cross-tolerance against anoxia in Arabidopsis. Plant Cell Environ 31, 1029–1037.
641 https://doi.org/10.1111/j.1365-3040.2008.01816.x
642 • Bi, C., Ma, Y., Wu, Z., Yu, Y.-T., Liang, S., Lu, K., Wang, X.-F., 2017. Arabidopsis ABI5 plays a role
643 in regulating ROS homeostasis by activating CATALASE 1 transcription in seed germination.
644 Plant Mol Biol 94, 197–213. https://doi.org/10.1007/s11103-017-0603-y
645 • Bouzid, M., He, F., Schmitz, G., Häusler, R.E., Weber, A.P.M., Mettler-Altmann, T., De Meaux, J.,
646 2019. Arabidopsis species deploy distinct strategies to cope with drought stress. Annals of
647 Botany 124, 27–40. https://doi.org/10.1093/aob/mcy237
648 • Casal, J.J., Balasubramanian, S., 2019. Thermomorphogenesis. Annu. Rev. Plant Biol. 70, 321–
649 346. https://doi.org/10.1146/annurev-arplant-050718-095919
650 • Chaves, M.M., Flexas, J., Pinheiro, C., 2009. Photosynthesis under drought and salt stress:
651 regulation mechanisms from whole plant to cell. Annals of Botany 103, 551–560.
652 https://doi.org/10.1093/aob/mcn125
653 • Chen, K., Huang, Y., Liu, C., Liang, Y., Li, M., 2021. Transcriptome Profile Analysis of Arabidopsis
654 Reveals the Drought Stress-Induced Long Non-coding RNAs Associated With Photosynthesis,
655 Chlorophyll Synthesis, Fatty Acid Synthesis and Degradation. Front. Plant Sci. 12, 643182.
656 https://doi.org/10.3389/fpls.2021.643182
657 • Choudhury, F.K., Rivero, R.M., Blumwald, E., Mittler, R., 2017. Reactive oxygen species, abiotic
658 stress and stress combination. Plant J 90, 856–867. https://doi.org/10.1111/tpj.13299
659 • Clauw, P., Coppens, F., De Beuf, K., Dhondt, S., Van Daele, T., Maleux, K., Storme, V., Clement,
660 L., Gonzalez, N., Inzé, D., 2015. Leaf Responses to Mild Drought Stress in Natural Variants of
661 Arabidopsis. Plant Physiology 167, 800–816. https://doi.org/10.1104/pp.114.254284

662 • Cohen, I., Zandalinas, S.I., Huck, C., Fritschi, F.B., Mittler, R., 2021. Meta-analysis of drought
663 and heat stress combination impact on crop yield and yield components. Physiol Plantarum
664 171, 66–76. https://doi.org/10.1111/ppl.13203
665 • Cornic, G., 2000. Drought stress inhibits photosynthesis by decreasing stomatal aperture – not
666 by affecting ATP synthesis. Trends in Plant Science 5, 187–188. https://doi.org/10.1016/S1360-
667 1385(00)01625-3
668 • Crevillén, P., Yang, H., Cui, X., Greeff, C., Trick, M., Qiu, Q., Cao, X., Dean, C., 2014. Epigenetic
669 reprogramming that prevents transgenerational inheritance of the vernalized state. Nature
670 515, 587–590. https://doi.org/10.1038/nature13722
671 • Cushman, J.C., Denby, K., Mittler, R., 2022. Plant responses and adaptations to a changing
672 climate. The Plant Journal 109, 319–322. https://doi.org/10.1111/tpj.15641
673 • De Smet, I., Quint, M., van Zanten, M., 2021. High and low temperature signalling and response.
674 Journal of Experimental Botany 72, 7339–7344. https://doi.org/10.1093/jxb/erab447
675 • De Smet, I., Xu, X., Praat, M., Pizzio, G., Jiang, Z., Driever, S., Wang, R., De Cotte, B.V., Villers, S.,
676 Gevaert, K., Leonhardt, N., Nelissen, H., Kinoshita, T., Vanneste, S., Rodriguez, P., Zanten, M.V.,
677 Vu, L., 2023. A conserved signaling axis integrates conflicting environmental drought and heat
678 signals to control stomatal aperture in plants (preprint). In Review.
679 https://doi.org/10.21203/rs.3.rs-3228667/v1
680 • Dekkers, B.J.W., He, H., Hanson, J., Willems, L.A.J., Jamar, D.C.L., Cueff, G., Rajjou, L., Hilhorst,
681 H.W.M., Bentsink, L., 2016. The Arabidopsis *DELAY OF GERMINATION 1* gene affects *ABSCISIC*
682 *ACID INSENSITIVE 5 (ABI5)* expression and genetically interacts with *ABI3* during Arabidopsis
683 seed development. Plant J 85, 451–465. https://doi.org/10.1111/tpj.13118
684 • Gao, J., Wang, M.-J., Wang, J.-J., Lu, H.-P., Liu, J.-X., 2022. bZIP17 regulates heat stress tolerance
685 at reproductive stage in Arabidopsis. aBIOTECH 3, 1–11. https://doi.org/10.1007/s42994-021-
686 00062-1
687 • Guo, Q., Li, X., Niu, L., Jameson, P.E., Zhou, W., 2021. Transcription-associated metabolomic
688 adjustments in maize occur during combined drought and cold stress. Plant Physiology 186,
689 677–695. https://doi.org/10.1093/plphys/kiab050

690 • Harb, A., Krishnan, A., Ambavaram, M.M.R., Pereira, A., 2010. Molecular and Physiological
691 Analysis of Drought Stress in Arabidopsis Reveals Early Responses Leading to Acclimation in
692 Plant Growth. Plant Physiology 154, 1254–1271. https://doi.org/10.1104/pp.110.161752
693 • He, K., Mei, H., Zhu, J., Qiu, Q., Cao, X., Deng, X., 2022. The histone H3K27 demethylase
694 REF6/JMJ12 promotes thermomorphogenesis in *Arabidopsis*. National Science Review 9,
695 nwab213. https://doi.org/10.1093/nsr/nwab213
696 • Järvi, S., Isojärvi, J., Kangasjärvi, S., Salojärvi, J., Mamedov, F., Suorsa, M., Aro, E.-M., 2016.
697 Photosystem II Repair and Plant Immunity: Lessons Learned from Arabidopsis Mutant Lacking
698 the THYLAKOID LUMEN PROTEIN 18.3. Front. Plant Sci. 7.
699 https://doi.org/10.3389/fpls.2016.00405
700 • Kataoka, R., Takahashi, M., Suzuki, N., 2017. Coordination between bZIP28 and HSFA2 in the
701 regulation of heat response signals in Arabidopsis. Plant Signaling & Behavior 12, e1376159.
702 https://doi.org/10.1080/15592324.2017.1376159
703 • Kong, R.S., Henry, H.A.L., 2016. Prior exposure to freezing stress enhances the survival and
704 recovery of *Poa pratensis* exposed to severe drought. American Journal of Botany 103, 1890–
705 1896. https://doi.org/10.3732/ajb.1600176
706 • Kopecká, R., Kameniarová, M., Černý, M., Brzobohatý, B., Novák, J., 2023. Abiotic Stress in Crop
707 Production. IJMS 24, 6603. https://doi.org/10.3390/ijms24076603
708 • Kulkarni, S.R., Vaneechoutte, D., Van de Velde, J., Vandepoele, K., 2018. TF2Network:
709 predicting transcription factor regulators and gene regulatory networks in Arabidopsis using
710 publicly available binding site information. Nucleic Acids Research 46, e31–e31.
711 https://doi.org/10.1093/nar/gkx1279
712 • Kumar, L., Chhogyel, N., Gopalakrishnan, T., Hasan, M.K., Jayasinghe, S.L., Kariyawasam, C.S.,
713 Kogo, B.K., Ratnayake, S., 2022. Climate change and future of agri-food production, in: Future
714 Foods. Elsevier, pp. 49–79. https://doi.org/10.1016/B978-0-323-91001-9.00009-8
715 • Larkindale, J., Hall, J.D., Knight, M.R., Vierling, E., 2005. Heat Stress Phenotypes of Arabidopsis
716 Mutants Implicate Multiple Signaling Pathways in the Acquisition of Thermotolerance. Plant
717 Physiology 138, 882–897. https://doi.org/10.1104/pp.105.062257
718 • Lê, S., Josse, J., Husson, F., 2008. FactoMineR: An R Package for Multivariate Analysis. J. Stat.
719 Soft. 25, 1–18. https://doi.org/10.18637/jss.v025.i01

720 • Lu, F., Cui, X., Zhang, S., Jenuwein, T., Cao, X., 2011. Arabidopsis REF6 is a histone H3 lysine 27
721 demethylase. Nat Genet 43, 715–719. https://doi.org/10.1038/ng.854
722 • Luo, F.-L., Nagel, K.A., Zeng, B., Schurr, U., Matsubara, S., 2009. Photosynthetic acclimation is
723 important for post-submergence recovery of photosynthesis and growth in two riparian
724 species. Annals of Botany 104, 1435–1444. https://doi.org/10.1093/aob/mcp257
725 • Masson-Delmotte, V., Zhai, P., Pirani, A., 2021. Climate change 2021: the physical science basis :
726 summary for policymakers : working group I contribution to the sixth Assessment report of the
727 Intergovernmental Panel on Climate Change. IPCC, Geneva, Switzerland.
728 • Méndez-Gómez, M., Sierra-Cacho, D., Jiménez-Morales, E., Guzmán, P., 2024. Modulation of
729 early gene expression responses to water deprivation stress by the E3 ubiquitin ligase ATL80:
730 implications for retrograde signaling interplay. BMC Plant Biology 24, 180.
731 https://doi.org/10.1186/s12870-024-04872-5
732 • Millenaar, F.F., Cox, M.C.H., Van Berkel, Y.E.M.D.J., Welschen, R.A.M., Pierik, R., Voesenek,
733 L.A.J.C., Peeters, A.J.M., 2005. Ethylene-Induced Differential Growth of Petioles in Arabidopsis.
734 Analyzing Natural Variation, Response Kinetics, and Regulation. Plant Physiology 137, 998–
735 1008. https://doi.org/10.1104/pp.104.053967
736 • Mittler, R., 2006. Abiotic stress, the field environment and stress combination. Trends in Plant
737 Science 11, 15–19. https://doi.org/10.1016/j.tplants.2005.11.002
738 • Mittler, R., Blumwald, E., 2010. Genetic Engineering for Modern Agriculture: Challenges and
739 Perspectives. Annual Review of Plant Biology 61, 443–462. https://doi.org/10.1146/annurev-
740 arplant-042809-112116
741 • Morales, A., de Boer, H.J., Douma, J.C., Elsen, S., Engels, S., Glimmerveen, T., Sajeev, N., Huber,
742 M., Luimes, M., Luitjens, E., Raatjes, K., Hsieh, C., Teapal, J., Wildenbeest, T., Jiang, Z., Pareek,
743 A., Singla-Pareek, S., Yin, X., Evers, J., Anten, N.P.R., van Zanten, M., Sasidharan, R., 2022. Effects
744 of sublethal single, simultaneous and sequential abiotic stresses on phenotypic traits of
745 Arabidopsis thaliana. AoB PLANTS 14, plac029. https://doi.org/10.1093/aobpla/plac029
746 • Mustroph, A., Zanetti, M.E., Jang, C.J.H., Holtan, H.E., Repetti, P.P., Galbraith, D.W., Girke, T.,
747 Bailey-Serres, J., 2009. Profiling translatomes of discrete cell populations resolves altered
748 cellular priorities during hypoxia in *Arabidopsis*. Proc. Natl. Acad. Sci. U.S.A. 106, 18843–18848.
749 https://doi.org/10.1073/pnas.0906131106

- Nadeem, H., Khan, A., Gupta, R., Hashem, M., ALAMRI, S., Siddiqui, M.A., Ahmad, F., 2023. Stress combination: When two negatives may become antagonistic, synergistic or additive for plants? Pedosphere 33, 287–300. https://doi.org/10.1016/j.pedsph.2022.06.031
- Nielsen, F., Mikkelsen, B.B., Nielsen, J.B., Andersen, H.R., Grandjean, P., 1997. Plasma malondialdehyde as biomarker for oxidative stress: reference interval and effects of life-style factors. Clinical Chemistry 43, 1209–1214. https://doi.org/10.1093/clinchem/43.7.1209
- Perdomo, J.A., Conesa, M.À., Medrano, H., Ribas-Carbó, M., Galmés, J., 2015. Effects of long-term individual and combined water and temperature stress on the growth of rice, wheat and maize: relationship with morphological and physiological acclimation. Physiol Plantarum 155, 149–165. https://doi.org/10.1111/ppl.12303
- Perrella, G., Bäurle, I., Van Zanten, M., 2022. Epigenetic regulation of thermomorphogenesis and heat stress tolerance. New Phytologist 234, 1144–1160. https://doi.org/10.1111/nph.17970
- Pradhan, G.P., Prasad, P.V.V., Fritz, A.K., Kirkham, M.B., Gill, B.S., 2012. Effects of drought and high temperature stress on synthetic hexaploid wheat. Functional Plant Biol. 39, 190. https://doi.org/10.1071/FP11245
- Prasch, C.M., Sonnewald, U., 2013. Simultaneous Application of Heat, Drought, and Virus to Arabidopsis Plants Reveals Significant Shifts in Signaling Networks. Plant Physiol. 162, 1849–1866. https://doi.org/10.1104/pp.113.221044
- Quint, M., Delker, C., Franklin, K.A., Wigge, P.A., Halliday, K.J., van Zanten, M., 2016. Molecular and genetic control of plant thermomorphogenesis. Nature Plants 2, 15190. https://doi.org/10.1038/nplants.2015.190
- Rankenberg, T., Geldhof, B., van Veen, H., Holsteens, K., Van de Poel, B., Sasidharan, R., 2021. Age-Dependent Abiotic Stress Resilience in Plants. Trends in Plant Science 26, 692–705. https://doi.org/10.1016/j.tplants.2020.12.016
- Rankenberg, T., van Veen, H., Sedaghatmehr, M., Liao, C.-Y., Devaiah, M.B., Stouten, E.A., Balazadeh, S., Sasidharan, R., 2024. Differential leaf flooding resilience in Arabidopsis thaliana is controlled by ethylene signaling-activated and age-dependent phosphorylation of ORESARA1. Plant Communications. https://doi.org/10.1016/j.xplc.2024.100848

- Rejeb, I., Pastor, V., Mauch-Mani, B., 2014. Plant Responses to Simultaneous Biotic and Abiotic Stress: Molecular Mechanisms. Plants 3, 458–475. https://doi.org/10.3390/plants3040458
- Richter, R., Bastakis, E., Schwechheimer, C., 2013. Cross-Repressive Interactions between SOC1 and the GATAs GNC and GNL/CGA1 in the Control of Greening, Cold Tolerance, and Flowering Time in Arabidopsis. Plant Physiology 162, 1992–2004. https://doi.org/10.1104/pp.113.219238
- Rivero, R.M., Mittler, R., Blumwald, E., Zandalinas, S.I., 2022. Developing climate-resilient crops: improving plant tolerance to stress combination. Plant J 109, 373–389. https://doi.org/10.1111/tpj.15483
- Rizhsky, L., Liang, H., Shuman, J., Shulaev, V., Davletova, S., Mittler, R., 2004. When Defense Pathways Collide. The Response of Arabidopsis to a Combination of Drought and Heat Stress. Plant Physiology 134, 1683–1696. https://doi.org/10.1104/pp.103.033431
- Samperna, S., Boari, A., Vurro, M., Salzano, A.M., Reveglia, P., Evidente, A., Gismondi, A., Canini, A., Scaloni, A., Marra, M., 2021. Arabidopsis Defense against the Pathogenic Fungus Drechslera gigantea Is Dependent on the Integrity of the Unfolded Protein Response. Biomolecules 11, 240. https://doi.org/10.3390/biom11020240
- Shabbir, R., Singhal, R.K., Mishra, U.N., Chauhan, J., Javed, T., Hussain, S., Kumar, S., Anuragi, H., Lal, D., Chen, P., 2022. Combined Abiotic Stresses: Challenges and Potential for Crop Improvement. Agronomy 12, 2795. https://doi.org/10.3390/agronomy12112795
- Shannon, P., Markiel, A., Ozier, O., Baliga, N.S., Wang, J.T., Ramage, D., Amin, N., Schwikowski, B., Ideker, T., 2003. Cytoscape: A Software Environment for Integrated Models of Biomolecular Interaction Networks. Genome Res. 13, 2498–2504. https://doi.org/10.1101/gr.1239303
- Sharma, P., Jha, A.B., Dubey, R.S., Pessarakli, M., 2012. Reactive Oxygen Species, Oxidative Damage, and Antioxidative Defense Mechanism in Plants under Stressful Conditions. Journal of Botany 2012, 1–26. https://doi.org/10.1155/2012/217037
- Shates, T.M., Sun, P., Malmstrom, C.M., Dominguez, C., Mauck, K.E., 2019. Addressing Research Needs in the Field of Plant Virus Ecology by Defining Knowledge Gaps and Developing Wild Dicot Study Systems. Front. Microbiol. 9, 3305. https://doi.org/10.3389/fmicb.2018.03305

807 • Sinha, R., Fritschi, F.B., Zandalinas, S.I., Mittler, R., 2021. The impact of stress combination on
808 reproductive processes in crops. Plant Science 311, 111007.
809 https://doi.org/10.1016/j.plantsci.2021.111007
810 • Skubacz, A., Daszkowska-Golec, A., Szarejko, I., 2016. The Role and Regulation of ABI5 (ABA-
811 Insensitive 5) in Plant Development, Abiotic Stress Responses and Phytohormone Crosstalk.
812 Frontiers in Plant Science 7.
813 • Suh, J.Y., Kim, W.T., 2015. Arabidopsis RING E3 ubiquitin ligase AtATL80 is negatively involved in
814 phosphate mobilization and cold stress response in sufficient phosphate growth conditions.
815 Biochemical and Biophysical Research Communications 463, 793–799.
816 https://doi.org/10.1016/j.bbrc.2015.06.015
817 • Suzuki, N., Rivero, R.M., Shulaev, V., Blumwald, E., Mittler, R., 2014. Abiotic and biotic stress
818 combinations. New Phytologist 203, 32–43. https://doi.org/10.1111/nph.12797
819 • Tricker, P.J., ElHabti, A., Schmidt, J., Fleury, D., 2018. The physiological and genetic basis of
820 combined drought and heat tolerance in wheat. Journal of Experimental Botany 69, 3195–
821 3210. https://doi.org/10.1093/jxb/ery081
822 • Van Dooren, T.J.M., Silveira, A.B., Gilbault, E., Jiménez-Gómez, J.M., Martin, A., Bach, L., Tisné,
823 S., Quadrana, L., Loudet, O., Colot, V., 2020. Mild drought in the vegetative stage induces
824 phenotypic, gene expression, and DNA methylation plasticity in Arabidopsis but no
825 transgenerational effects. J Exp Bot 71, 3588–3602. https://doi.org/10.1093/jxb/eraa132
826 • Van Veen, H., Mustroph, A., Barding, G.A., Vergeer-van Eijk, M., Welschen-Evertman, R.A.M.,
827 Pedersen, O., Visser, E.J.W., Larive, C.K., Pierik, R., Bailey-Serres, J., Voesenek, L.A.C.J.,
828 Sasidharan, R., 2013. Two Rumex Species from Contrasting Hydrological Niches Regulate
829 Flooding Tolerance through Distinct Mechanisms. The Plant Cell 25, 4691–4707.
830 https://doi.org/10.1105/tpc.113.119016
831 • van Veen, H., Vashisht, D., Akman, M., Girke, T., Mustroph, A., Reinen, E., Hartman, S., Kooiker,
832 M., van Tienderen, P., Schranz, M.E., Bailey-Serres, J., Voesenek, L.A.C.J., Sasidharan, R., 2016.
833 Transcriptomes of Eight Arabidopsis thaliana Accessions Reveal Core Conserved, Genotype-
834 and Organ-Specific Responses to Flooding Stress. Plant Physiology 172, 668–689.
835 https://doi.org/10.1104/pp.16.00472

836 • Vashisht, D., Hesselink, A., Pierik, R., Ammerlaan, J.M.H., Bailey-Serres, J., Visser, E.J.W.,
837 Pedersen, O., Van Zanten, M., Vreugdenhil, D., Jamar, D.C.L., Voesenek, L.A.C.J., Sasidharan, R.,
838 2011. Natural variation of submergence tolerance among *Arabidopsis thaliana* accessions.
839 New Phytologist 190, 299–310. https://doi.org/10.1111/j.1469-8137.2010.03552.x
840 • Verelst, W., Bertolini, E., De Bodt, S., Vandepoele, K., Demeulenaere, M., Enrico Pè, M., Inzé,
841 D., 2013. Molecular and Physiological Analysis of Growth-Limiting Drought Stress in
842 Brachypodium distachyon Leaves. Molecular Plant 6, 311–322.
843 https://doi.org/10.1093/mp/sss098
844 • Verhoeven, A., Kloth, K.J., Kupczok, A., Oymans, G.H., Damen, J., Rijnsburger, K., Jiang, Z.,
845 Deelen, C., Sasidharan, R., van Zanten, M., van der Vlugt, R.A.A., 2023. Arabidopsis latent virus
846 1, a comovirus widely spread in *Arabidopsis thaliana* collections. New Phytologist 237, 1146–
847 1153. https://doi.org/10.1111/nph.18466
848 • Wang, T., Huang, S., Zhang, A., Guo, P., Liu, Y., Xu, C., Cong, W., Liu, B., Xu, Z., 2021. JMJ17–
849 WRKY40 and HY5–ABI5 modules regulate the expression of ABA-responsive genes in
850 Arabidopsis. New Phytologist 230, 567–584. https://doi.org/10.1111/nph.17177
851 • Wickham, H., 2009. ggplot2: Elegant Graphics for Data Analysis. Springer New York, New York,
852 NY. https://doi.org/10.1007/978-0-387-98141-3
853 • Wu, H.-Y., Liu, M.-S., Lin, T.-P., Cheng, Y.-S., 2011. Structural and Functional Assays of AtTLP18.3
854 Identify Its Novel Acid Phosphatase Activity in Thylakoid Lumen. Plant Physiology 157, 1015–
855 1025. https://doi.org/10.1104/pp.111.184739
856 • Yamaguchi, N., Matsubara, S., Yoshimizu, K., Seki, M., Hamada, K., Kamitani, M., Kurita, Y.,
857 Nomura, Y., Nagashima, K., Inagaki, S., Suzuki, T., Gan, E.-S., To, T., Kakutani, T., Nagano, A.J.,
858 Satake, A., Ito, T., 2021. H3K27me3 demethylases alter HSP22 and HSP17.6C expression in
859 response to recurring heat in Arabidopsis. Nat Commun 12, 3480.
860 https://doi.org/10.1038/s41467-021-23766-w
861 • Yang, X., Zou, F., Zhang, Y., Shi, J., Qi, M., Liu, Y., Li, T., 2022. NaCl Pretreatment Enhances the
862 Low Temperature Tolerance of Tomato Through Photosynthetic Acclimation. Frontiers in Plant
863 Science 13, 891697. https://doi.org/10.3389/fpls.2022.891697
864 • Zandalinas, S.I., Balfagón, D., Arbona, V., Gómez-Cadenas, A., Inupakutika, M.A., Mittler, R.,
865 2016a. ABA is required for the accumulation of APX1 and MBF1c during a combination of water

deficit and heat stress. Journal of Experimental Botany 67, 5381–5390. https://doi.org/10.1093/jxb/erw299

- Zandalinas, Sara I., Fichman, Y., Devireddy, A.R., Sengupta, S., Azad, R.K., Mittler, R., 2020. Systemic signaling during abiotic stress combination in plants. Proceedings of the National Academy of Sciences 117, 13810–13820. https://doi.org/10.1073/pnas.2005077117
- Zandalinas, S.I., Fritschi, F.B., Mittler, R., 2021. Global Warming, Climate Change, and Environmental Pollution: Recipe for a Multifactorial Stress Combination Disaster. Trends in Plant Science 26, 588–599. https://doi.org/10.1016/j.tplants.2021.02.011
- Zandalinas, Sara I, Fritschi, F.B., Mittler, R., 2020. Signal transduction networks during stress combination. Journal of Experimental Botany 71, 1734–1741. https://doi.org/10.1093/jxb/erz486
- Zandalinas, S.I., Mittler, R., 2022. Plant responses to multifactorial stress combination. New Phytologist 234, 1161–1167. https://doi.org/10.1111/nph.18087
- Zandalinas, S.I., Rivero, R.M., Martínez, V., Gómez-Cadenas, A., Arbona, V., 2016b. Tolerance of citrus plants to the combination of high temperatures and drought is associated to the increase in transpiration modulated by a reduction in abscisic acid levels. BMC Plant Biol 16, 105. https://doi.org/10.1186/s12870-016-0791-7
- Zhang, H., Sonnewald, U., 2017. Differences and commonalities of plant responses to single and combined stresses. Plant J 90, 839–855. https://doi.org/10.1111/tpj.13557
- Zhang, H., Zhao, Y., Zhu, J.-K., 2020. Thriving under Stress: How Plants Balance Growth and the Stress Response. Developmental Cell 55, 529–543. https://doi.org/10.1016/j.devcel.2020.10.012
- Zhou, R., Yu, X., Ottosen, C.-O., Rosenqvist, E., Zhao, L., Wang, Y., Yu, W., Zhao, T., Wu, Z., 2017. Drought stress had a predominant effect over heat stress on three tomato cultivars subjected to combined stress. BMC Plant Biol 17, 24. https://doi.org/10.1186/s12870-017-0974-x
- Zhou, Y., Zhou, B., Pache, L., Chang, M., Khodabakhshi, A.H., Tanaseichuk, O., Benner, C., Chanda, S.K., 2019. Metascape provides a biologist-oriented resource for the analysis of systems-level datasets. Nat Commun 10, 1523. https://doi.org/10.1038/s41467-019-09234-6